REGENERATION

Inhalable SPRAY nanoparticles by modular peptide assemblies reverse alveolar inflammation in lethal Gram-negative bacteria infection

Dinghao Chen[1,2,3], Ziao Zhou[2,3], Nan Kong[2,3], Tengyan Xu[2,3], Juan Liang[2,3], Pingping Xu[2,3], Bingpeng Yao[4], Yu Zhang[2,3], Ying Sun[4], Ying Li[2,3], Bihan Wu[2,3], Xuejiao Yang[2,3], Huaimin Wang[2,3]*

Current pharmacotherapy remains futile in acute alveolar inflammation induced by Gram-negative bacteria (GNB), eliciting consequent respiratory failure. The release of lipid polysaccharides after antibiotic treatment and subsequent progress of proinflammatory cascade highlights the necessity to apply effective inflammation management simultaneously. This work describes modular self-assembling peptides for rapid anti-inflammatory programming (SPRAY) to form nanoparticles targeting macrophage specifically, having anti-inflammation and bactericidal functions synchronously. SPRAY nanoparticles accelerate the self-delivery process in macrophages via lysosomal membrane permeabilization, maintaining anti-inflammatory programming in macrophages with efficacy close to T helper 2 cytokines. By pulmonary deposition, SPRAY nanoparticles effectively suppress inflammatory infiltration and promote alveoli regeneration in murine aseptic acute lung injury. Moreover, SPRAY nanoparticles efficiently eradicate multidrug-resistant GNB in alveoli by disrupting bacterial membrane. The universal molecular design of SPRAY nanoparticles provides a robust and clinically unseen local strategy in reverse acute inflammation featured by a high accumulation of proinflammatory cellularity and drug-resistant bacteria.

INTRODUCTION

As the final stage of unmanaged alveolar inflammation, acute lung injury (ALI), featuring hypoxemia and bilateral pulmonary infiltrates, results in respiratory failure with 38.5% mortality (*1*, *2*). Gram-negative bacteria (GNB) infection is one of ALI's most common and notorious risk factors. Its outer membrane component, lipopolysaccharide (LPS), rapidly activates the Toll-like receptor 4 (TLR4)/CD14 signaling cascade in alveolar macrophage (AlvM) and polarizes it to the M1 phenotype. Subsequently, the expansion of proinflammatory cellularity in lung edema further leads to epithelial and endothelial damage (*3*), causing edema accumulation and impairment of gas exchange (*4*). The swift progress of ALI necessitates concerted therapy, including oxygenation and ventilatory (*5*), plus most essential antibacterial therapy and certain inflammation constriction (*6*). Clinically, the long-term systemic dosing of antibiotics is applied to combat lethal infection caused by GNB but results in poor pulmonary drug accumulation (*7*), of which the growing number of drug-resistant strains may further compromise the efficacy (*8*). In addition, the action of antibiotics, e.g., ampicillin, cotrimoxazole, and azithromycin, increases the LPS release from GNB to deteriorate lung injury or cause severe side effects such as endotoxin shock (*9*), emphasizing the anti-inflammatory therapy in GNB-induced ALI. However, clinically available immunosuppressive-based pharmacotherapy is frequently feeble because of (i) uncleared therapeutic outcomes (e.g., glucocorticoids) (*10*), (ii) incompetence in constructing a regenerative environment (*11*), and (iii) the reduction of host defense to existing infection (*12*). For example, the popular anticytokine therapies (e.g., tocilizumab) only neutralize proinflammatory cytokines or related receptors but may render a more susceptible respiratory tract to invading or colonized pathogens (*13*).

To overcome these predicaments, an inhalable nanoparticle orchestrated anti-inflammatory, antibacterial, and regenerative functions to secure the recovery process in pulmonary lesions while favoring the local delivery to maximize therapy effectiveness. Notably, microenvironment predominated by anti-inflammatory macrophages (M2) is necessary for the recovery of acute inflammation by inaugurating downstream protective and regenerative processes (*14*), thus acting as a universal anti-inflammatory target. However, the direct AlvM targeting to induce M2 activation is currently very limited in GNB-infected lung (*15*). Because regenerative medicine modulates macrophages by the delivery of drugs (*16*, *17*), nucleic acid (*18*) or stem cells (*19*) were still in its preclinical stage. The self-functioned biomaterials to modulate macrophage are specifically designed for topical use on epidermal (*20*, *21*), cardiovascular (*22*), and tumor (*23*) rather than respiratory tract, and thus may not be suitable for the harsh alveolar environment. Recent studies indicate that the M2 macrophage polarization and bacteria eradication could be simultaneously achieved by cationic peptides (*24*), including human host defense peptides (e.g., HD6 defensin) (*25*), naturally occurring antimicrobial peptides (e.g., melittin), or other synthetic peptides (*26*). However, the immunomodulation of most cationic peptides is too diverse to satisfy the clinical requirements (*27*).

This work reports a category of nanoparticles composed of modular self-assembly peptides for rapid anti-inflammatory programming (SPRAY) that compulsively reverse acute proinflammatory response by reshaping macrophages. We constructed SPRAY by conjugating a membrane-permeable motif (MPM) with a cationic peptide sequence to trigger anti-inflammatory functions. MPM comprised a biphenyl group (Bip) and two phenylalanine residues (FF). MPM assists the self-assembly process by dexterity to enhance π-π stacking (fig. S1) (*28*, *29*). Further, it interacts with the lipid bilayer, potentiating the membrane

[1]Department of Chemistry, Zhejiang University, Hangzhou 310027, Zhejiang Province, China. [2]Key Laboratory of Precise Synthesis of Functional Molecules of Zhejiang Province, Department of Chemistry, School of Science, Westlake University, Hangzhou 310030, China. [3]Westlake Laboratory of Life Sciences and Biomedicine, 18 Shilongshan Road, Hangzhou 310024, Zhejiang Province, China. [4]Departments of Pharmacology and Department of Respiratory and Critical Care Medicine of the Second Affiliated Hospital, Zhejiang University, School of Medicine, Key Laboratory of Respiratory Disease of Zhejiang Province, Hangzhou, China.
*Corresponding author. Email: wanghuaimin@westlake.edu.cn

disruption under local accumulation (*30*–*32*). The cationic sequence is truncated from existing peptides or designed sophisticatedly (Fig. 1A). To prove our conception, a short library of candidates was engineered and screened to generate the optimal SPRAY, called BLKR, by selecting a truncated sequence from antimicrobial peptide SAAP-148 (*33*), termed LKR (table S1). Our result suggested that MPM conjugation helps with the formation of BLKR nanoparticles (SPRAY-BLKR-NPs) and enhances cytoplasmic delivery of BLKR for anti-inflammatory M2 polarization and inhibition of M1-related signaling. Moreover, MPM renders SPRAY-BLKR-NPs to efficiently eradicate multidrug-resistant *Escherichia coli* (*MRE*) in mice through membrane disruption in injured airspace and reverses ALI within a week. Together, we envisioned SPRAY nanoparticles as the express medication for treating GNB-induced ALI and hold enormous translational potential.

RESULTS

The optimization of SPRAY to complete M2 macrophage polarization

To screen the optimal SPRAY, we applied the initial turn of screening by analysis of CD206 expression level in peptide-treated macrophage because CD206 represents the M2 phenotype polarization (Fig. 1B). Through the quantification of the percentage of $CD206^+$ cells in total $CD11b^+F4/80^+$ bone marrow–derived macrophages (BMDMs), BKII, BLKR, BRLI, and BKRA ranked the top four anti-inflammatory potencies, with the overall M2 macrophage percentage at near 28.84, 28.67, 24.32, and 16.83% (Fig. 1C and fig. S2), respectively.

Subsequently, the second turn of screening shall identify general cytotoxicity of candidates against various cells that might be exposed to SPRAY during in vivo absorption and distribution process, including the epithelial cells, immune cells, and red blood cells (RBCs). Hemolysis is the primary concern during the translation of cationic antimicrobial peptides. Thus, we next performed an imperative examination of the hemolytic effect led by peptide candidates (Fig. 1F). BKII and BLKR exhibited no detectable hemolytic activity even at 256 μM [16-fold of minimal inhibitory concentration (MIC)]. BRLI is eliminated from the candidate pool because of its 7.49% hemolysis rate at 128 μM. Moreover, epithelial cells and macrophages are the most ubiquitous two classes of pulmonary cells to uptake incoming peptides or nanoparticles through the respiratory tract (*34*, *35*). After demonstrating BLKR and BKII have no notable cytotoxicity toward human bronchial epithelial cells (BEAS-2B) (Fig. 1D), we also showed that only BLKR renders the eventual viability larger than 80% in the human monocytes (THP-1) (Fig. 1E), the results of which are extremely encouraging because macrophages are more susceptible. Moreover, BLKR showed no significant cytotoxicity when treating another two kinds of epithelial cells [human embryonic kidney (HEK) 293T and HS-5 (human marrow stromal cells)] and antigen-presenting cells (RAW264.7, DC2.4), further demonstrating the cytocompatibility of BLKR (fig. S3).

Last, considering a large portion of ALI was raised following GNB infection, the optimal SPRAY candidate shall exert vigorous antibacterial ability as a necessary simultaneous therapy. *E. coli*, the common cause of GNB-induced nosocomial pneumonia, was selected as the model pathogen (*36*, *37*). The MIC value of BLKR against *MRE* is 16 μM. Admittedly, BKII failed to show antibacterial activity even at 256 μM and therefore was not chosen despite its strong anti-inflammatory ability (Fig. 1G).

On the basis of above results, BLKR is distinguished for its combinational embracing of M2 polarization ability, biocompatibility, and bacterial eradication and would be comprehensively investigated in the following experiments. We further demonstrated that the anti-inflammatory property of this optimal SPRAY is highly sequence specific, because two scrambled sequences of BLKR, BWLR and BVRR, failed to significantly improve CD206 expression in BMDMs (fig. S6, A to C), even though their uptake quantity in BMDMs is on a similar scale as that of BLKR (fig. S6, D to F), respectively.

The optimal SPRAY induces anti-inflammatory M2 macrophage in vitro

We used BMDMs to examine the influence of BLKR on the M2 polarization and the corresponding mechanism. The flow cytometry results (Fig. 2A and fig. S38) revealed that LKR failed to activate the desired M2 phenotype. However, nearly 27% of BMDMs in the treatment of BLKR transformed into $CD206^+$ M2 macrophage, suggesting MPM is an essential framework for anti-inflammatory programming. Notably, interleukin-4 (IL-4) and IL-10 generate 33% M2 macrophages. Meanwhile, LPS rather than BLKR or LKR eventually rendered more than 80% of $CD86^+$ macrophage in the total population (Fig. 2B and fig. S4). F-actin (Fig. 2C) staining indicated that BMDMs presented round-shaped morphology at the M0 state. Upon the treatment of BLKR, it transformed into a long fusiform structure, which is consistent with the observation by the stimulation of the IL-4 and IL-10. The immunofluorescence staining revealed that CD206 protein is highly expressed on the cell membrane and partially in the cytoplasm under the treatment of BLKR, suggesting that BLKR shares similar M2 polarization ability as T helper 2 (T_H2) cytokines do. Real-time quantitative polymerase chain reaction (qPCR) analysis indicates that BLKR significantly heightened the mRNA levels of several emblematic anti-inflammatory markers, including Arginase-1 (Arg-1), CD206, YM-1, and Fizz-1 (*38*) (Fig. 2D). Because the T_H2 cytokines secreted by M2 macrophage are regulatory to numerous tissue-repair responses during the inflammation (*39*), we further tested the levels of T_H1/T_H2 cytokines in BMDM culture supernatant by the enzyme-linked immunosorbent assay (ELISA). Compared to untreated cells, BLKR up-regulated IL-4, IL-10, and IL-5 levels by 7.9-, 4.3-, and 2.0-fold (Fig. 2E, and fig. S5), respectively. The treatment of BLKR does not affect the secretion of interferon-γ (IFN-γ) and down-regulated the production of tumor necrosis factor–α (TNF-α) by 1.9-fold (fig. S5). These results indicate that BLKR might play a role in tissue repair during inflammation.

SPRAY-induced transcriptome reprogramming to control M2 polarization

To unravel the possible biological signal transduction uniquely manipulated by BLKR. We conducted the transcriptomics analysis on the LKR- or BLKR-treated BMDMs. Among all detected genes, BLKR and LKR shared 11,754 genes, and the rest are singly distributed in certain groups (fig. S7). The principal components analysis and M-versus-A (MA) plotting demonstrated the essential transcriptome reprogramming in response to BLKR treatment, as the samples treated with either LKR or BLKR are well splitted with markedly different regulations on gene pattern (figs. S8 and S9). To further explore the function affected by BLKR treatment, we performed Gene Ontology (GO) enrichment analysis. In detail, up to 196 differentially expressed genes were eminently T_H1/T_H2 cytokines biosynthesis process, namely, the production of IL-4, IL-5, IL-12, and IFN-γ (Fig. 2F). Then, we concluded the top 12 significant signaling pathways affected by the BLKR according to Kyoto Encyclopedia of Genes and Genomes (KEGG) enrichment analysis

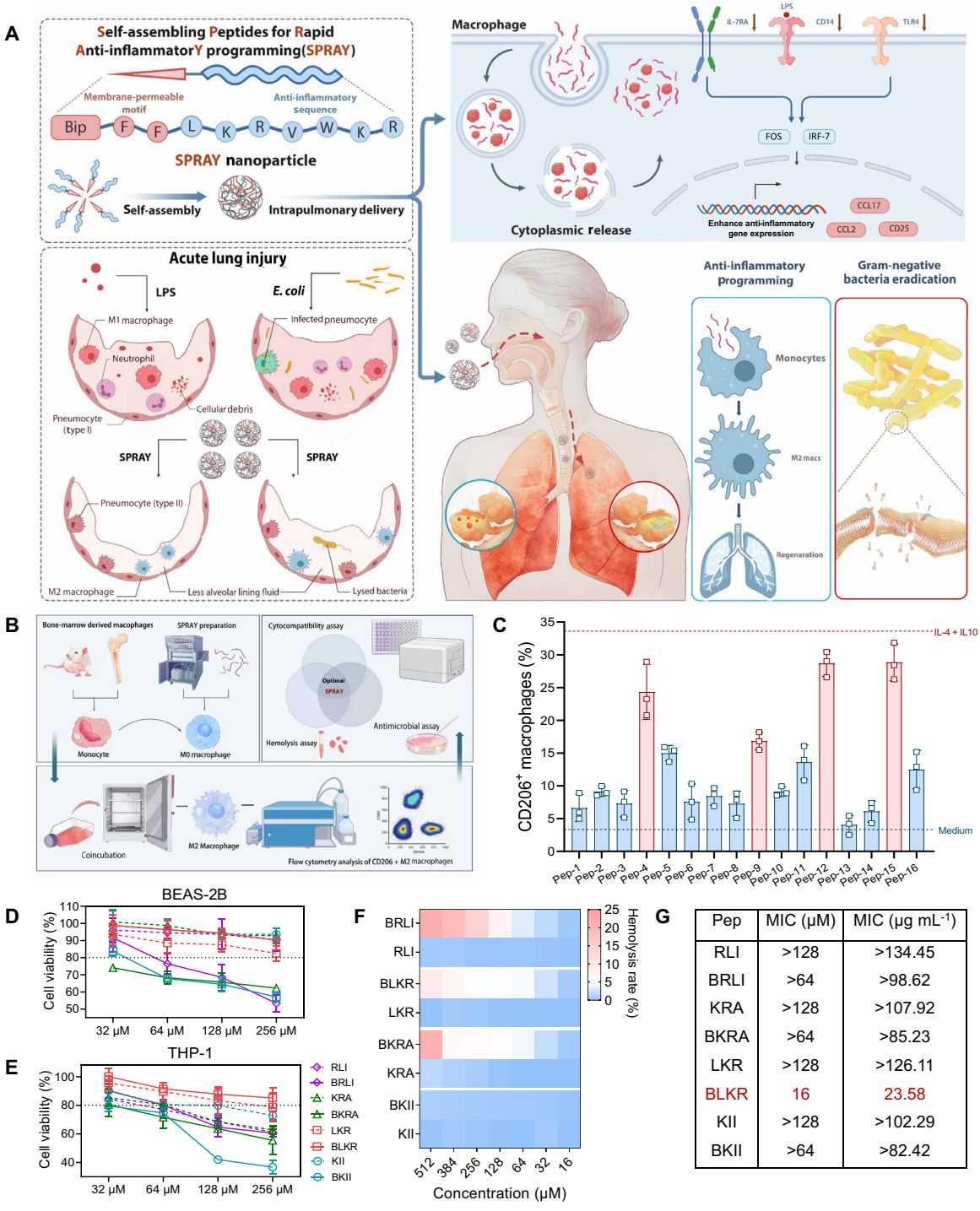

Pep	MIC (μM)	MIC (μg mL^{-1})
RLI	>128	>134.45
BRLI	>64	>98.62
KRA	>128	>107.92
BKRA	>64	>85.23
LKR	>128	>126.11
BLKR	16	23.58
KII	>128	>102.29
BKII	>64	>82.42

Fig. 1. The molecular design and the discovery of a biocompatible SPRAY with dual M2 macrophage polarization and antibacterial activity. (**A**) BLKR was screened out as the optimal SPRAY that is comprised of an MPM and anti-inflammatory heptapeptide, exerting two prominent therapeutic roles: (i) SPRAY nanoparticles achieve anti-inflammatory immune programming in AlvMs through enhanced cytoplasmic delivery and amplifies the M2-related signaling transduction. (ii) SPRAY nanoparticles disrupt the membrane integrity of GNB and switch the inflammatory state when treating GNB-induced ALI. (**B**) The schematic illustration for the screening processes of optimal SPRAY. (**C**) The percentage of CD206$^+$ M2 macrophage after peptide treatment at the concentration of 16 μM. The dotted line in blue noted the percent of CD206$^+$ cells treated by blank culture medium. The dotted line in red noted the percentage of CD206$^+$ cells treated by IL-4 and IL-10. The peptides ranked in the top four are shown in red. $n = 3$, mean ± SD. (**D** and **E**) The cytocompatibility of anti-inflammatory SPRAY candidates to lung epithelial cells [Beas-2B; (D)] and macrophage [THP-1; (E)]. (**F**) The heatmap plotting of the hemolysis rate of anti-inflammatory SPRAY candidates. The up-limitation of the acceptable hemolysis rate was set as 5% (white). Data are presented as mean value, $n = 9$. (**G**) The MIC value against *MRE* of anti-inflammatory SPRAY candidates, $n = 3$ biologically replicates. The MIC value (in micrograms per milliliter) in the third column was calculated from the value in the second column (in micromolar).

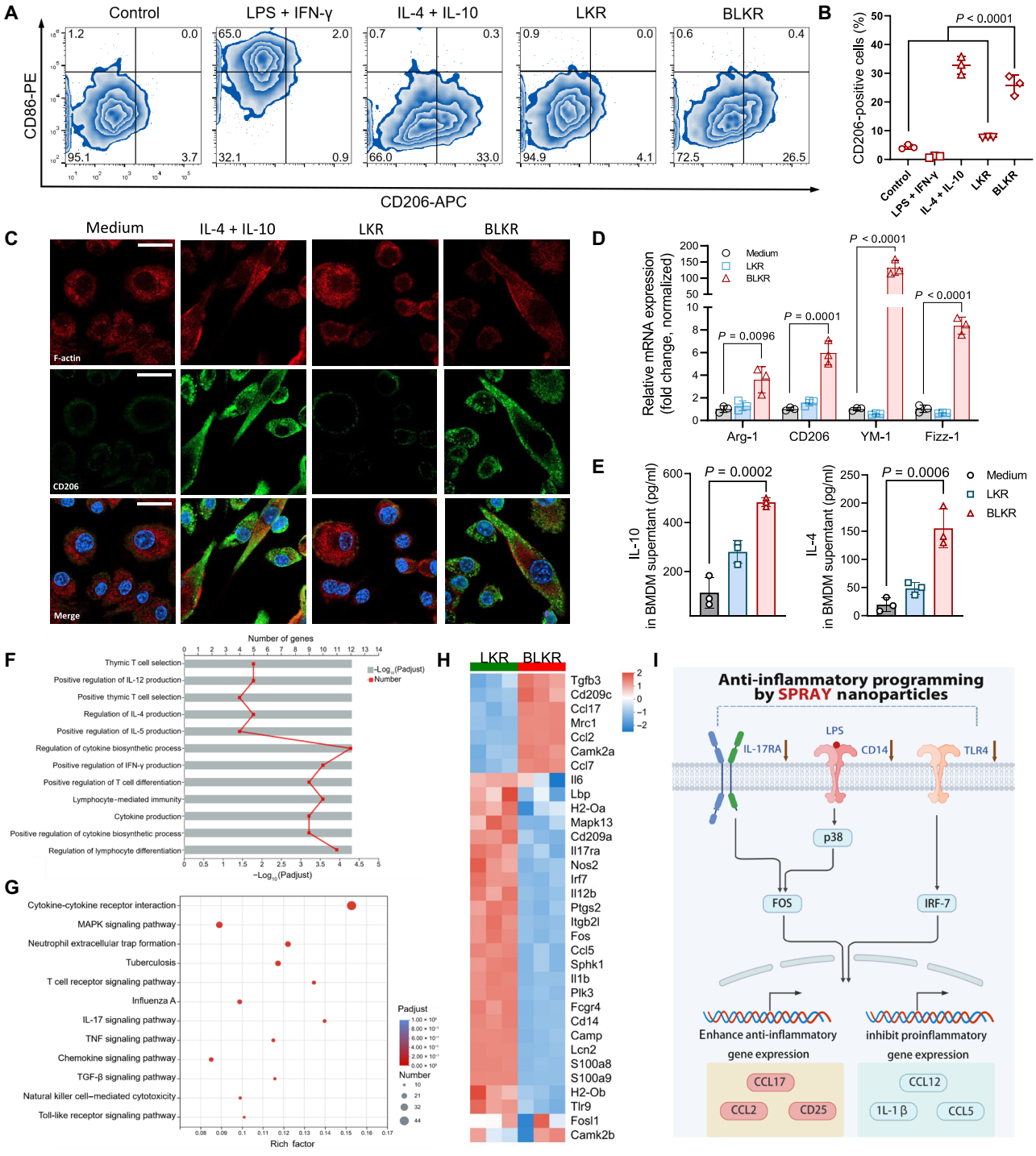

Fig. 2. The N-terminal modification enables optimal SPRAY to potentiate the M2-type macrophage polarization. (**A**) The flow cytometry analyzing the CD206 and CD86 expression levels demonstrates that BLKR rather than LKR induces M2 macrophage. (**B**) The quantification of M2 macrophage percentage ($CD11b^+F4/80^+CD206^+$ cells) in (A), $n = 3$, mean ± SD. (**C**) Representative CLSM images of BMDMs treated by indicated peptide (16 μM) for 24 hours (green, CD206; red, F-actin; blue, DAPI). Scale bar, 20 μm. (**D**) Real-time qPCR analysis of mRNA expression of M2-related marker (Arg-1, CD206, YM-1, and Fizz-1), $n = 3$, mean ± SD. (**E**) The ELISA test of the T_H2 cytokines levels (IL-10, left; IL-4, right) in the BMDM supernatant, $n = 3$, mean ± SD. (**F**) The GO enrichment analysis in BLKR group compared with LKR group. (**G**) KEGG pathway enrichment analysis for BLKR versus LKR group. (**H**) Heatmap plotting for clustering 33 differentially expressed genes under LKR and BLKR treatments in IL-17, MAPK, and TLR pathways. $n = 3$. (**I**) Schematic representation of the IL-17, MAPK, and TLR signaling cascade regulated by BLKR to trigger M2 macrophage polarization and inhibit M1 phenotype polarization. IRF-7, interferon regulatory factor-7; FOS, Fos proto-oncogene; CD14, cluster of differentiation 14 for LPS binding; p38, p38 mitogen-activated protein kinase, CCL17, C-C motif chemokine ligand 17; CCL2, C-C motif chemokine ligand 2; CD25, interleukin 2 receptor subunit alpha; CCL5, C-C motif chemokine ligand 5. Statistical analysis in (B), (D), and (E) was conducted using one-way analysis of variance (ANOVA).

(BLKR versus LKR) (Fig. 2G). Seeking the regulatory functions of essential genes, we subsequently plotted the clustering of up to 33 differentially expressed genes to comprehensively reveal that the key immunoreactions are mainly enriched in IL-17, mitogen-activated protein kinase (MAPK), and TLR pathways. In general, the genes related to T_H2 responses are up-regulated to varying degrees, while the expression of most genes in TLR signaling is inhibited (Fig. 2H). Herein, we normalized the expression level of related genes in IL-17, MAPK, and TLR signaling (fig. S10). Specifically, the lower expression of IL-17Ra further caused the down-regulation of FOS through the MAPK pathway, then triggered downstream expression of CD25 and CCL17 to potentiate T_H2 cell responses (*40*, *41*), and suppress T_H17 cell responses through IL-17 signaling pathway. Moreover, we found BLKR stimulated the downstream expression of CCL2, demonstrating M2 phenotype may be enabled through the increasing level of immunosuppressive CCL2 expression (*42*, *43*) (Fig. 2I).

Besides promoting M2 macrophage-related T_H2 immunoreactions, BLKR also blocked the proinflammatory signal transduction. CD14 is a well-documented LPS-binding protein to activate TLR4. The mRNA expression level of CD14 under BLKR treatment is lowered by 1.8-fold, suggesting that the cellular sensitivity to LPS is down-regulated (fig. S10). To verify this, we find the impotence of LPS for further M1 repolarization in BMDMs after the preincubation of BLKR at 16 or 128 μM. Notably, such inhibition cannot be completed by using IL-4 and IL-10 (fig. S11).

Characterization of the self-assembly property of SPRAY

The critical micelle concentration (CMC) values of BLKR and LKR is 89 and 2560 μM (Fig. 3A), respectively, suggesting that the MPM enables original LKR to acquire an enhanced self-assembly ability by precisely increasing the hydrophobicity at the N terminus. The circular dichroism (CD) indicates that MPM conjugation alters the secondary structure of peptide to potentiate the formation of nanoparticles. The original negative peak at 203 nm transformed into a positive peak at 188 nm together with a negative peak at 209 nm.

As shown by transmission electronic microscope (TEM; Fig. 3C), BLKR forms nanoparticles, SPRAY-BLKR-NPs, with a diameter around 20 nm in physiological conditions at 128 μM, which could be favored for intrapulmonary delivery to reach the lower respiratory tract. However, the addition of LKR in the same condition results in an undetectable nanostructure, further demonstrating the importance of MPM in the formation of nanoparticles. We further demonstrated that SPRAY-BLKR-NPs retained desired particle properties in injured alveolar environment for up to 1.5 hours, which promisingly ensures the efficient uptake process during the real therapy (fig. S12). Moreover, the accelerated storage experiment proved that BLKR retained strong self-assembly property after being exposed to refrigeration, high temperature, and light exposure, evidenced by corresponding nonsignificantly changed reconstituted particle sizes (fig. S13).

SPRAY renders the enhanced cytoplasmic delivery

Confocal laser scanning microscopy (CLSM; Fig. 3D) shows that the green fluorescence from fluorescein isothiocyanate (FITC)–BLKR colocalized with the red fluorescence from Lyso-Tracker, implying that BLKR is uptaken by BMDMs through endocytosis and trapped in the endosomes at the first 1 hour. After incubating for 4 hours, more green fluorescence appeared in the cytoplasm, suggesting that the previously trapped BLKR started to escape from the endosome. Twelve hours after the coincubation, more peptides entered into the cytoplasm and distributed in the cytoplasm in a dotted pattern. No noticeable green fluorescence of FITC-LKR appeared in cells at all tested time points (fig. S14). The quantified mean fluorescent intensity measured by flow cytometry of BLKR is about 30- and 195-fold larger than the LKR group and control group, respectively (Fig. 3, F and G). These results suggested that the nanoparticles facilitate the cytoplasmic delivery of functional anti-inflammatory peptide sequence by enhancing the cellular endocytosis and accelerating endosomal escape through latent membrane destabilization.

We next used well-established endocytic inhibitors to investigate the endocytosis mode involved in the BLKR uptake by BMDMs. The addition of Filipin III reduces the percentage of FITC-positive cells from 95.28 to 73.68% (Fig. 3H), while leading to a 43.01% loss of BLKR uptake quantified by FITC intensity, suggesting that caveolae-mediated endocytosis contributes to the cellular uptake of BLKR (fig. S15). In addition, ethyl-isopropyl-amiloride (EIPA) and chlorpromazine (CPZ), inhibitors for macropinocytosis/clathrin-mediated endocytosis, also led to the decrease of cellular uptake of BLKR by 22.14 and 24.47%, respectively. We further demonstrated that such multiple endocytic pathways of BLKR in BMDMs by the combination of different inhibitors. Notably, when Filipin III, CPZ, and EIPA were applied simultaneously, only 33.47% of cells had positive BLKR signals. The absence of Filipin III significantly lowered the inhibition rate as the combination use of CPZ and EIPA reached 70.58% SPRAY-positive cells (fig. S16). These results together illustrate the cellular uptake of BLKR undergoes the aforementioned different endocytic pathways. Bio-EM provides direct evidence for the intracellular fate of BLKR (Fig. 3E). Within the commencing 15 min, BLKR entered the macrophage, which was verified by the observation that peptide assemblies accumulated on the cell surface and were incorporated into the emerging vesicles. Forty-five minutes later, the BLKR assembles were sparsely distributed in endosomes, then further condensed in the endosomes at 2 hours, reflected by the pattern within the endosome gradually darkened. Notably, the structure of the endosomal membrane destructed at 4 hours to render the cytoplasmic release (Fig. 3I).

SPRAY nanoparticles accumulated in injured lung through targeting AlvMs

On the basis of the above encouraging results, we evaluated the capacity of SPRAY-BLKR-NPs to reverse the pulmonary aseptic inflammation after establishing the ALI mice model by the intratracheal injection of LPS (10 mg kg^{-1}) in mice on day 0 (Fig. 4A). The local administration of our nanoparticle was selected for its maximized lung retention, meanwhile simulating the actual medication process based on the inhalation of anti-inflammatory agents in patients with ALI. Therefore, the pulmonary biodistribution of SPRAY was checked first. Our CLSM results confirmed that SPRAY-BLKR-NPs were not distributed in airway epithelial cells or endothelial cells but predominantly in the immune cells that infiltrated in alveoli. (fig. S17). Thus, we next comprehensively investigate the uptake status of BLKR in various types of pulmonary immune cells in injured lung. The uptake of SPRAY-BLKR-NPs mainly occurred in myeloid cells, in which nearly 51.01% of AlvMs uptook SPRAY particles within 1 hour. Less than 10% of neutrophils, dendritic cells, and eosinophils show positive BLKR signals. In contrast, lymphoid cells, including T cells and B cells, show negligible BLKR uptake (Fig. 4G and fig. S39). Encouragingly, we further directly visualized the colocalization of SPRAY-BLKR-NPs with $CD68^+$ pulmonary macrophages in the alveolar space at 1 hour after administration (Fig. 4F). In comparison, LKR exhibited extremely little accumulation in injured lung tissue, witnessed

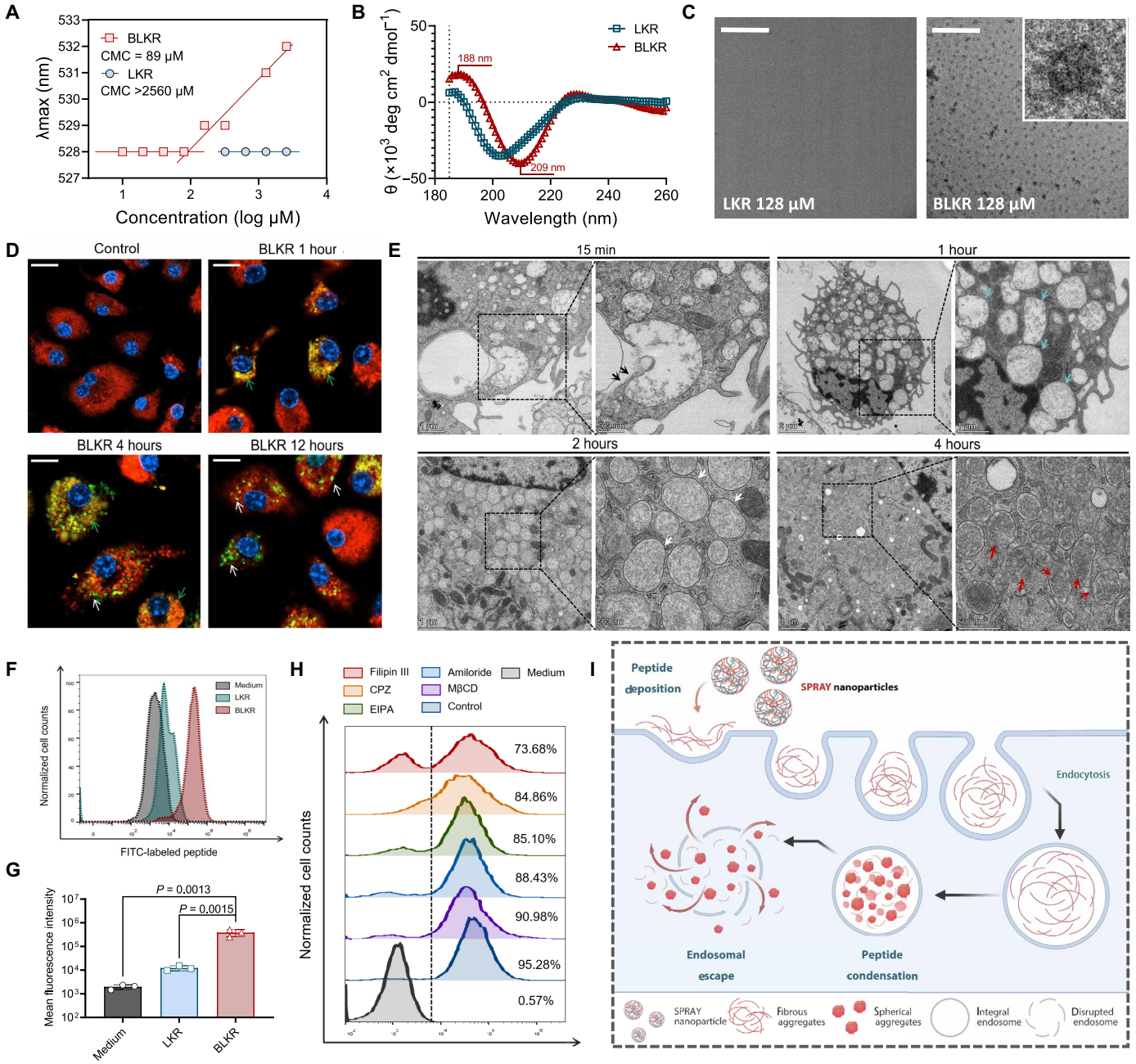

Fig. 3. The N-terminal modification renders self-assembly to induce nanoparticle formation and cytoplasmic release of functional anti-inflammatory sequence. (**A**) The CMC measurement for BLKR and LKR. (**B**) The CD spectra of BLKR peptide. (**C**) The representative TEM images of the self-assembly structures of LKR and BLKR (128 μM). (**D**) The representative CLSM images demonstrating the uptake behavior of BLKR in BMDMs. Blue, DAPI-stained nuclei; red, lysotracker; green, FITC-labeled BLKR. Scale bar, 100 μm. The peptide trapped in the endosome was noted with green arrow. The peptide that escaped from the endosome was indicated with white arrow. (**E**) The representative Bio-EM images of BMDMs treated by BLKR for 15 min, 1 hour, 2 hours, and 4 hours. The endocytosis process was noted with black arrow. The peptide distributed in the endosome was indicated with blue arrow. The integral endosomal membrane was noted with white arrow. The disruption of the endosomal membrane was marked with red arrow. (**F**) The histogram of FITC fluorescence intensity of BMDMs treated by BLKR or LKR for 1 hour. (**G**) The quantification of mean fluorescence intensity of FITC-labeled peptide in (F). Data are presented as mean ± SD, $n = 3$ biologically replicates. (**H**) The histogram plotting the FITC signal of BMDMs treated by FITC-labeled BLKR (16 μM) for 15 min in absence (Control) or presence of endocytosis inhibitor MβCD (5 mM), Amiloride (50 μM), EIPA (ethyl-isopropyl-amiloride; 50 μM), CPZ (chlorpromazine; 40 μM), and Filipin III (5 μg ml^{-1}). (**I**) The scheme of SPRAY's cellular uptake processes and cytoplasmic release. Statistical analysis in (G) was conducted using one-way ANOVA.

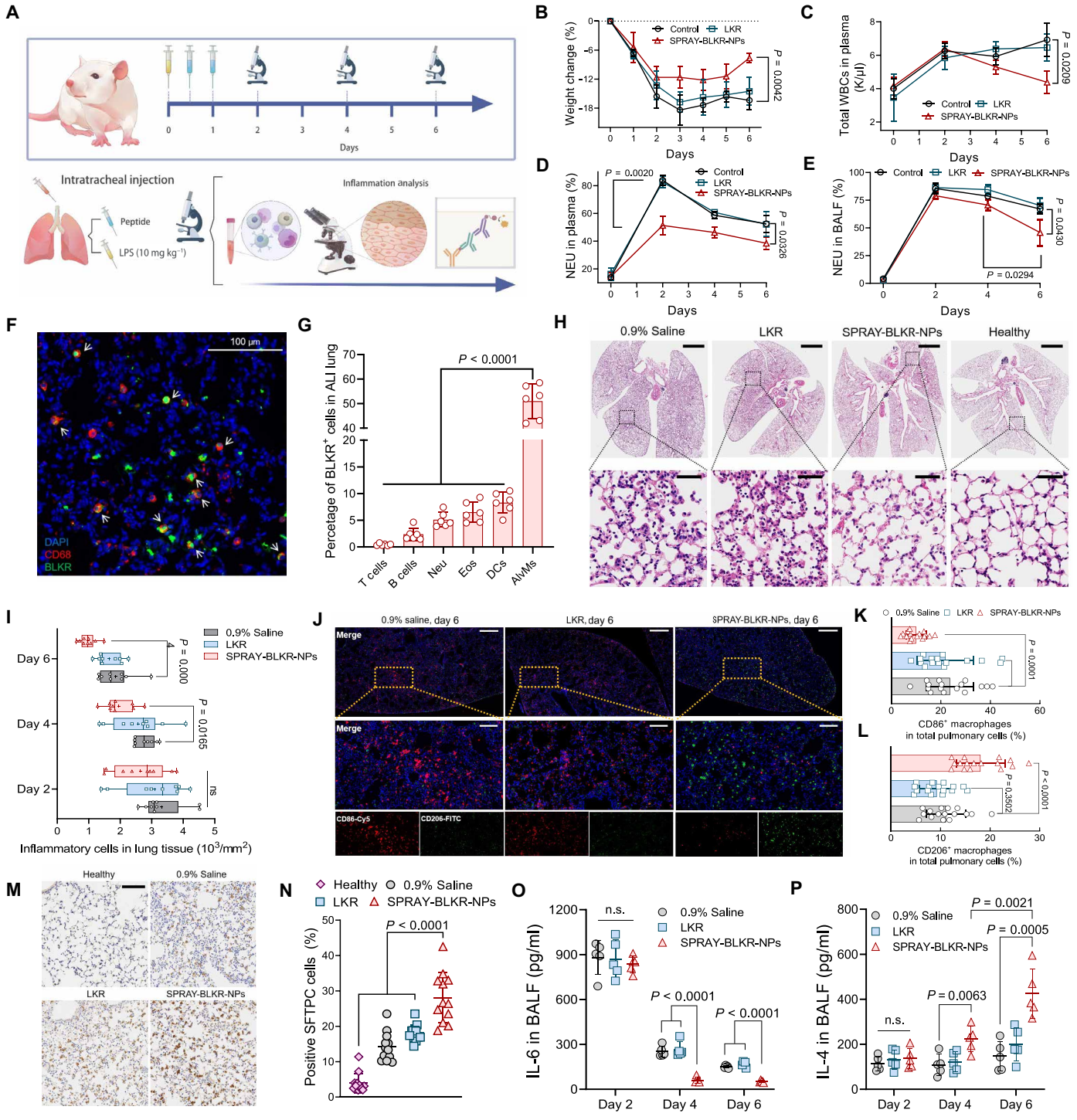

Fig. 4. SPRAY nanoparticles are promising to reverse the inflammation in LPS-induced ALI via M2 macrophage polarization. (**A**) Scheme illustrating the medication schedule for ALI mice. (**B**) Body weight monitoring. (**C** to **E**) Hematology monitoring of plasma white blood cell (WBC) counts (C), percentage of NEU in plasma (D) and BALF (E), $n = 3$. WBC, white blood cells; NEU, neutrophils. (**F**) Biodistribution of BLKR in injured lung at 1 hour after administration. Scale bar, 100 μm. Red, CD68; green, FITC-BLKR; blue, DAPI. (**G**) Uptake distribution of SPRAY-BLKR-NPs in various lung immune cell types, $n = 3$. AlvMs, alveolar macrophages; DCs, dendritic cells; Eos, eosinophils. (**H**) Representative images of lung H&E staining on day 6 (wide view, scale bar, 2.5 mm; enlarged region, scale bar, 50 μm). (**I**) Quantification of inflammatory cells in alveoli, min to max; +, mean value. (**J**) Representative immunofluorescence staining of pulmonary macrophages on day 6. Wide view, scale bar, 400 μm; enlarged region, scale bar, 10 μm (red, CD86; green, CD206; blue, DAPI). (**K** and **L**) Percentage of $CD86^+$ (K) and $CD206^+$ macrophages (L) in total pulmonary cells. (**M**) Representative immunohistochemistry staining of SFTPC (20× field) on day 6. Scale bar, 100 μm. SFTPC, surfactant protein C. (**N**) Percentage of $SFTPC^+$ cells in total pulmonary cells, $n = 3$. (**O** and **P**) The IL-6 (O) and IL-4 (P) concentration in BALF on day 6, $n = 5$. Data in (B) to (E), (G), (I), (K), (L), and (N) to (P) are presented as means ± SD. Statistical analysis was conducted using one-way ANOVA.

by its virtually undetectable fluorescence in both healthy and injured lung.

We next measured the overall pulmonary retention of peptide molecules in injured lung on the single dosage of SPRAY-BLKR-NPs (fig. S18). Herein, more than 83.54% of dosed BLKR remained in the lung tissue at 15 min after administration. Moreover, the pulmonary area under the curve of BLKR is more than 47.90 and 154.13 times larger than that in liver or kidney within 24 hours. These results indicated that BLKR is predominantly accumulated and metabolized in lung tissue. Near 10% BLKR was left in entire respiratory tract at 12 hours after administration, suggesting that a twice-administration (every 12 hours) schedule is needed to maintain pulmonary peptide content.

Besides, a small amount of BLKR also accumulated in liver at the first 1 hour and then gradually decreased, suggesting that the liver could also metabolize BLKR that leaked through the air-blood barrier in alveoli. Our further measurement indicated BLKR is metabolizable by liver microsome in human, monkey, dog, rat, and mouse, with related half-life ranging from 4.04 to 37.94 min (table S5).

SPRAY nanoparticles inhibit the proinflammatory status in aseptic ALI

On the basis of our screening of effective dosage range, SPRAY-BLKR-NPs was dosed at 0.38 mg kg^{-1} (128 μM, 50 μl) twice a day (every 12 hours) on day 1 for treating aseptic ALI (fig. S19 and Fig. 4A). In subsequent daily clinical inspection, with the loss of 14% body weight by day 2, the weight turning points for mice that received SPRAY-BLKR-NPs occurred on day 3, as the weight maintained then elevated on day 5. The mice that received LKR lost nearly 18% body weight on day 3 and failed to show recovery later (Fig. 4B).

The composition of leukocytes in bronchoalveolar lavage fluid (BALF) and plasma exhibits the fundamental status of the pulmonary migration of inflammatory cells (Fig. 4, C to E, and fig. S20). On day 2, we found that plasma leukocytes in mice from all groups elevated to nearly 6 K μl^{-1}, while the down-regulation occurred on day 6 (Fig. 4C). The plasma neutrophils only count for 51.36% of total leukocytes, 1.6-fold smaller than Saline group (Fig. 4D). This result indicated that neutrophil mobilization might be partially inhibited by SPRAY-BLKR-NP treatment. Mitigation also occurred in mice received saline and LKR. However, the plasma neutrophil percentage in the SPRAY-BLKR-NP group was still significantly lower than the level in other two groups on day 6, respectively. There was a distinct delay in the mitigation of pulmonary neutrophil migration. Neutrophils predominantly accumulated in the lung lumen during the acute phase of ALI, of which the percentages in all groups were higher than 70% until day 4. On day 6, we lastly found that only the BALF neutrophil percentage in the SPRAY-BLKR-NP group dropped to 45.8%, suggesting that the proinflammatory immune status was principally inhibited (Fig. 4E).

The histological analysis revealed that alveolar inflammatory cell infiltration occurred intensively on day 2 as the critical feature for the onset of ALI. The mice received SPRAY-BLKR-NPs showed the most considerable diminution of alveolar inflammatory cell count from day 2 to day 6 (Fig. 4H and figs. S21 and S22). By quantifying the counts of inflammatory cells in the alveoli, the infiltration condition in SPRAY-BLKR-NP group started to mitigate at day 4, as the SPRAY-BLKR-NP treatment lowered the cell counts to nearly 1.4-fold more diminutive than Saline group. Such mitigation became more significant on day 6 because SPRAY-BLKR-NPs decreased the inflammatory cell counts in alveoli to about 1.9-fold compared to LKR group (Fig. 4I).

Pulmonary M2 macrophage polarization by SPRAY-BLKR-NPs expedited tissue regeneration

To directly verify the efficient inflammatory mitigation that was observed mainly contributed to the M2 macrophage polarization inducing through SPRAY-BLKR-NP treatment, we used immunofluorescent staining of lung tissues to differentiate $CD86^+$ M1 macrophage and $CD206^+$ M2 macrophage (Fig. 4J). The mice received ineffectual anti-inflammatory therapy, including saline and LKR, to maintain the substantial accumulation of M1 macrophage in the lung tissue. In contrast, the SPRAY-BLKR-NPs reduced the M1 macrophage percentage from 23% to nearly 10%, indicating that the progression of the inflammatory state is largely inhibited (Fig. 4K). Moreover, SPRAY-BLKR-NPs rendered the M2 macrophage to dominate the entire macrophage population as its percentage was boosted from 9 to 18% (Fig. 4L). Such a switch in dominated macrophage phenotype proves that SPRAY-BLKR-NPs is promising to reverse the proinflammatory state in ALI to a regenerative anti-inflammatory state. Furthermore, this reduction of the M1 macrophage population resulted in the descending pulmonary IL-6 level. All three groups show similar BALF IL-6 levels larger than 400 pg ml^{-1} on day 2, then gradually decreased, in which the SPRAY-BLKR-NPs most timely accomplished local IL-6 level below 65 pg ml^{-1} on day 4 (Fig. 4O). Notably, IL-6 is mainly secreted by the macrophages or neutrophils in pulmonary tissue and then enters blood circulation. The systemic cytokine fluctuation might be less sensitive than the local site. Our tracking of systemic IL-6 levels also clued to such mitigation of inflammation by witnessing the significant reduction in serum IL-6 level only at day 4 (fig. S23A).

The differentiation of M2 macrophage would secrete IL-4, a key T_H2 cytokine (*44*), to trigger a regenerative microenvironment for alveolar epithelial stem cell proliferation (*45*) and type II pneumocyte differentiation (*46*). We subsequently confirmed that the establishment of such pulmonary regenerative environment as BALF IL-4 level in SPRAY-BLKR-NP group is near 222 pg ml^{-1}, about two times higher than mice received LKR. These distinctions were further expanded, as evidenced by the finding that BALF IL-4 elevated to 426 pg ml^{-1} at day 6, which is threefold larger than the LKR group (Fig. 4P). We also observed a steady plasma IL-4 level lower than 100 pg ml^{-1} at tested time points (fig. S23B), suggesting that the switch of inflammation status mainly occurred locally in lung tissue without a systematic manner. During recovery, M2 macrophages facilitate the proliferation and differentiation of type II pneumocytes to secrete lung surfactant protein C (SFTPC) as a protective agent to accelerate tissue regeneration (*47*, *48*). As shown in Fig. 4M, SPRAY-BLKR-NPs induced the most obvious proliferation of type II pneumocytes on day 6. In detail, type II pneumocytes accounted for approximately 28% of total pulmonary cells in SPRAY-BLKR-NP group, which was at least 1.5-fold larger than the level in the Saline or LKR group. Notably, less than 5% of cells are demonstrated to be SFTPC positive in healthy mice lungs (Fig. 4N).

Pulmonary monocyte infiltration regulated by optimal SPRAY in healthy lung

To study the potential immunomodulatory effect on monocytes led by BLKR in healthy mice lungs. The healthy mice are administrated with BLKR at different dosages twice and then analyzed 24 hours later for acute immunomodulation inspection (Fig. 5A). First, we find no elevation of monocyte percentage in peripheral blood (Fig. 5F) at all the tested concentrations. Next, the potential monocyte infiltration caused by BLKR in the lung parenchyma is investigated. CD64 and tyrosine-protein kinase Mer (MERTK) were selected

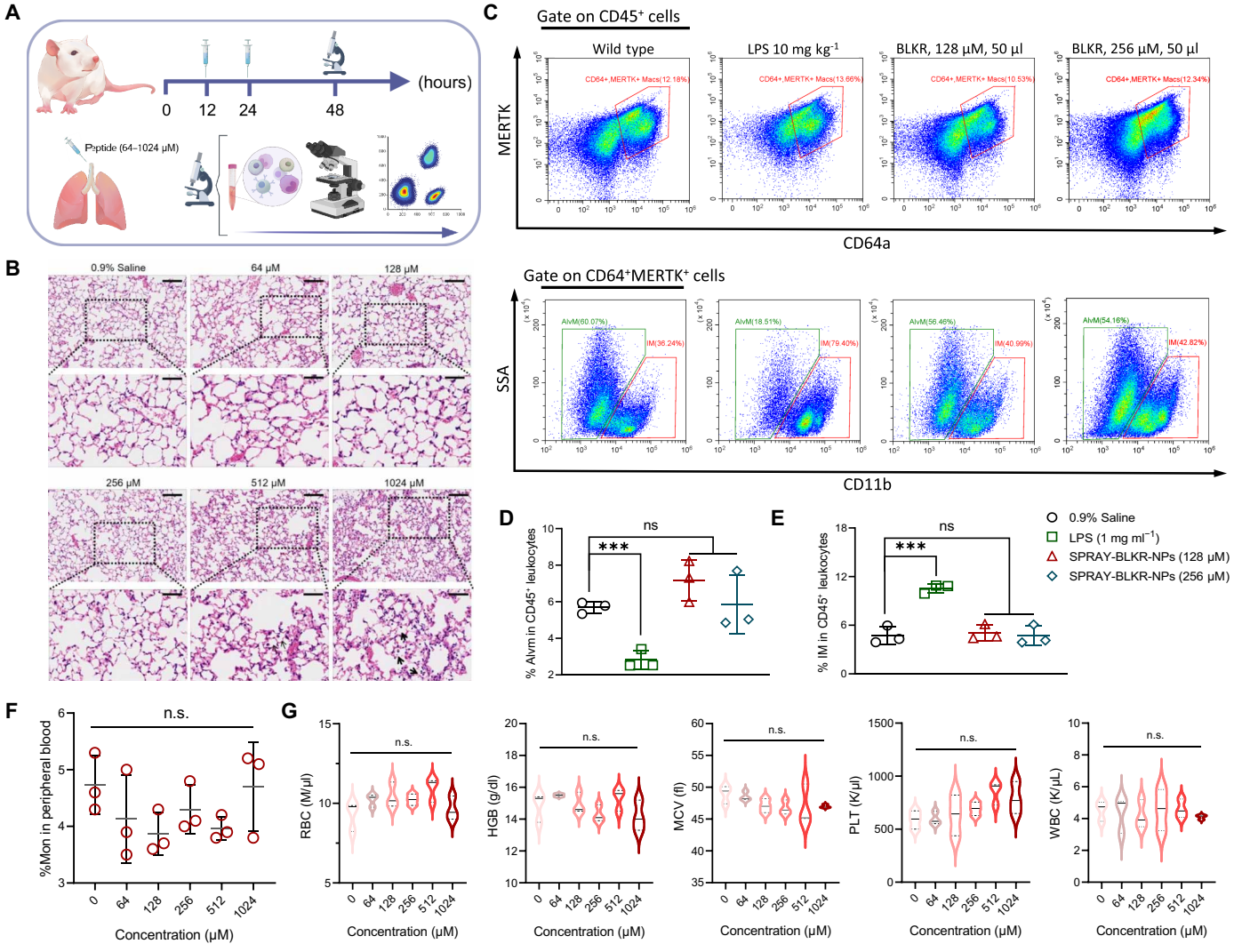

Fig. 5. Potential pulmonary macrophage infiltration and adverse effects of optimal SPRAY in healthy mice. (**A**) The experiment designed to analyze macrophage recruitment in healthy mice. (**B**) The representative images of H&E staining of lung tissue of healthy mice received BLKR at indicated dosage. Representative areas were shown in the first row (scale bar, 100 μm). The enlargement of focused area (black frame) was shown in the second row (scale bar, 50 μm). The infiltrated immune cells were noted using black arrow. (**C**) The flow cytometry analysis of IMs and tissue-resident AlvMs infiltration in pulmonary tissue induced by peptide treatment. The pulmonary macrophage was gated by CD64a and MERTK from $CD45^+$ cells. (Upper row). The IMs and AlvMs were then gated using CD11b from $CD45^+CD64^+MERTK^+$ cells (lower row). (**D** and **E**) The quantification of AlvMs (D) and IMs (E) in $CD45^+$ leukocytes. $n = 3$ mice per group, mean ± SD. (**F**) The percentage of monocyte (MON) in total leukocytes in peripheral blood. $n = 3$ mice per group, mean ± SD. (**G**) Blood parameters at 24 hours after the BLKR administration. $n = 5$ mice, violin plot, quartiles are shown in dotted lines, mean values are shown in solid lines. WBC, white blood cell; HGB, hemoglobin; MCV, mean corpuscular volume; PLT, platelets. Statistical analysis was conducted using one-way ANOVA.

to gate the pulmonary monocyte from $CD45^+$ pulmonary leukocytes. Then, CD11b was applied to differentiate AlvMs and interstitial macrophages (IMs) (fig. S40). The positive control, LPS, significantly lifted the IM percentage to nearly 70% in total $CD45^+CD64^+MERTK^+$ monocytes (Fig. 5C), suggesting pronounced monocyte infiltration. In contrast, the mice lung treated with BLKR (128 or 256 μM) showed a similar level of $CD45^+CD64^+MERTK^+$ monocyte as Saline group. Besides, the percentage of IMs and AlvMs maintained the same after the treatment with BLKR in the total lung $CD45^+$ leukocytes (Fig. 5D).

The histological analysis got a similar conclusion because no monocyte infiltration was observed in the alveolar site after BLKR treatment (128 or 256 μM). Notably, inflammatory cell infiltration occurred in lung when treated with higher concentrations (512 or 1204 μM). These results together suggested that BLKR is safe to use locally and without altering monocyte infiltration at concentrations up to 256 μM (Fig. 5B).

Biosafety evaluation of SPRAY nanoparticles

The results also confirmed that such short-term (1 day, two doses) exposure to SPRAY-BLKR-NPs would not lead to hemolysis, anemia, or systemic inflammation as similar plasma levels of RBC counts, hemoglobin, mean corpuscular volume, and platelets were found in the mice receiving different dosages of SPRAY-BLKR-NPs.

Besides, SPRAY-BLKR-NPs did not alter the plasma leukocyte level (Fig. 5G) or cause acute injury in the main organs, suggesting the excellent biocompatibility of our system (fig. S24).

We also performed the safety profile of SPRAY-BLKR-NPs under long-term (14-day) exposure to respiratory tract (fig. S25A). No significant abnormality in blood parameters was detected during or after the consecutive 14-day dosing period (fig. S25, B to F). Liver and kidney function remained unaffected throughout the evaluating period, which might be due to the fact that BLKR is mainly distributed in the lungs rather than the liver and kidneys (fig. S25, G to K). Further histological inspection confirmed the absence of any sign of acute injury in the main organs at 2 weeks after discontinuation of nanoparticle exposure (fig. S25L).

Potential damage to the respiratory system under long-term exposure was particularly focused (fig. S26A). We applied three times lung function tests on days 6, 15, and 27, respectively, to reveal similar levels of inspiratory capacity, forced expiratory volume (FEV0.2), resistance, static compliance, forced vital capacity and elastance in nanoparticle-treated mice as healthy mice did (fig. S26, B to G). Further BALF examination of pro/anti-inflammatory cytokines levels (fig. S26, H and I) and lung hematoxylin and eosin (H&E) staining (fig. S26J) suggest the nonoccurrence of T_H1/T_H2-related inflammation or fibrosis.

SPRAY nanoparticles exert promising bactericidal activity

Besides the rapid activation of TL4 signaling cascade in immune cells, GNB could also directly injure the integrity of alveolar endothelium to increased permeability that allows liquid to migrate from the lung endothelium to the interstitial alveolar lumen (*3*). During the progress of GNB colonization, type II pneumocytes are weakened to absorb the excessive apical fluid (*4*). Moreover, GNB and toxins could leak into blood circulation because of increased endothelial permeability and eventually lead to devasting sepsis. Thus, we next comprehensively evaluate the antibacterial activity of SPRAY-BLKR-NPs.

In vitro experiments show that SPRAY-BLKR-NPs killed 99.961% *MRE* and 99.997% methicillin-resistant *Staphylococcus aureus* (*MRSA*) at 128 μM (Fig. 6A and fig. S27). Then, we investigated whether SPRAY-BLKR-NPs is qualified for specialized pulmonary bacterial eradication. In injured alveoli, accumulated phospholipids and proteins provide nonspecific adhesion and compromise the efficacy of cationic agents. Thus, competent antibacterial agents shall especially tolerate the harsh environment of the lungs. We mimic the healthy and injured alveoli microenvironment using the BALF extracted from untreated mice and mice with aseptic ALI, in which SPRAY-BLKR-NPs reached anti-*MRE* efficiency at 98.83% in healthy BALF and 96.41% in ALI BALF (Fig. 6B). Moreover, during pulmonary infection, the changed airway microenvironment would enhance the bacteria attachment on epithelium to lastly form biofilms, which essentially prevents the normal phagocytosis by macrophages, facilitates the growth of drug resistance, and severely deteriorates the injury condition. The results suggested that SPRAY-BLKR-NPs eradicated both the *MRE* and *MRSA* biofilm as evidenced by the live/dead staining using SYTO9/Propidium Iodide (PI) (Fig. 6C and fig. S28). The crystal violet staining further showed that BLKR lowered relative biomass by 2.06-fold in *MRE* (Fig. 6D) and 1.62-fold in *MRSA* (fig. S29). These results proved the feasibility of using SPRAY-BLKR-NPs to combat local pulmonary bacteria eradication.

The membrane disruption mechanism ensures bacteria eradication by SPRAY nanoparticles

SEM imaging indicated that the healthy *E. coli* has long cylindrical morphology with slight wrinkles on its integral cell membrane. In contrast, most bacterial cell membranes become disintegrated (white arrow) after SPRAY-BLKR-NP treatment, while some bacteria directly lysed into cell debris (black arrow), suggesting SPRAY-BLKR-NPs induce membrane disruption to eradicate *MRE* (Fig. 6E). Such disruption was also observed in *MRSA* (fig. S30). To prove that such membrane disruption is the predominant mechanism, we used *N*-phenylnaphthalen-1-amine (NPN) assay to perform membrane integrity analysis. The results show a marked boost of normalized NPN fluorescence in SPRAY-*MRE* treated by SPRAY-BLKR-NPs compared to untreated *MRE* (Fig. 6F).

The membrane potential examination using a voltage-sensitive dye $DiSC_3(5)$ indicated a sharp uplift of $DiSC_3(5)$ fluorescence intensity within the first 5 min after the addition of SPRAY-BLKR-NPs (Fig. 6G), clearly affirming the close interaction between BLKR with the components of bacterial membrane. LNPs composed of 1,2-distearoyl-sn-glycero-3-phosphoethanolamine (PE), 1,2-dioleoyl-sn-glycero-3-phosphoglycerol (PG), and cardiolipin (DPG) (79:17:4) were extruded to investigate the detailed interaction mode between GNB membrane with BLKR. CD showed the appearance of standard β sheet secondary structure (positive peak at 196 nm; negative peak at 214 nm) once BLKR binds to the artificial GNB membrane (fig. S31), indicating that BLKR undergoes reassembling process and conformational change to form ordered nanostructure during bacteria eradication. After verifying membrane disruption, we further explored the potential intracellular disorder the peptide leads. According to the Bio-EM images of the bacterial section, the appearance of membrane disruption is confirmed in *MRE* or *MRSA* (Fig. 6H and fig. S32) in SPRAY-BLKR-NP group. Cytoplasmic morphology changes are absent, suggesting that membrane disruption is the main contributor to overall antibacterial efficacy. In addition, such physical antibacterial mechanism expanded the application of SPRAY to kill other GNB strains, such as *Klebsiella pneumoniae* and *Pseudomonas aeruginosa* (tables S3 and S4) and may help to delay the development of drug resistance (*49*).

Nanoparticles of BLKR rescue mice by in vivo *MRE* eradication

Etiological studies revealed that bacterial infection is one of the most prevalent causes of lung injury. GNB could cause lobar pneumonia (*50*), in which the invading bacteria multiply in the alveoli site and release toxins to provoke ALI (*51*). After establishing bacteria-induced ALI by local infection with a lethal dose of *MRE* in pulmonary tissue, we first screen the therapeutic dosage range by administrating the mice with SPRAY-BLKR-NPs every 12 hours during the first 2 days, in which the dosage at 0.76 mg kg^{-1} (256 μM, 50 μl) per administration ensured the primary *MRE* eradication adequacy and the following recovery process to rescue the overall survival condition (fig. S33, A to E). According to the plotting of pulmonary *MRE* burden, the first dose of SPRAY-BLKR-NPs reached 96.03% *MRE* eradication efficiency compared to Saline group, whose second dose of SPRAY-BLKR-NPs further eliminated nearly 78.39% of residual *MRE* to approach the 98.76% anti-*MRE* efficiency (Fig. 6J). Thus, the first two doses of BLKR rather than LKR are competent for diminishing pulmonary *MRE* burden. There is no significant difference in the pulmonary *MRE* quantity between the first and second doses of saline, demonstrating that the self-immunity could not eradicate resident *MRE* on day 1.

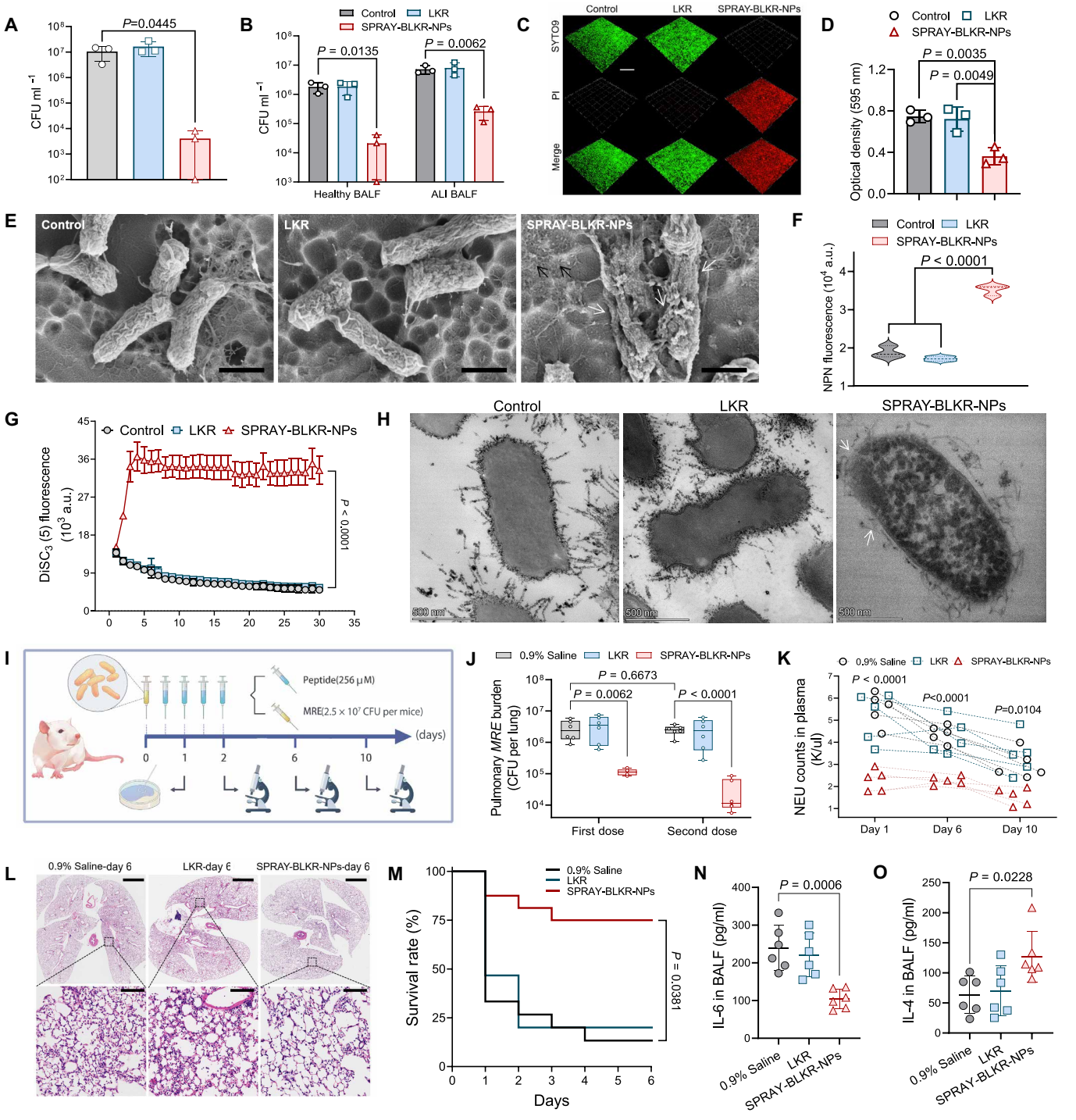

Fig. 6. SPRAY-BLKR-NPs exert bacteriacidal activity through membrane disruption and rescue mice from *MRE*-induced ALI. (**A**) In vitro viability of *MRE* after peptide (128 μM) treatment. (**B**) Ex vivo assay evaluating the anti-*MRE* activity of peptide (256 μM) in alveolar environments. (**C**) Representative CLSM imaging of *MRE* biofilm treated by indicated peptide (green, SYTO9; red, PI). Scale bar, 160 μm. (**D**) Crystal violet assay of *MRE* biofilm, mean ± SD, $n = 3$. (**E**) Representative SEM images of peptide-treated *MRE*. The membrane disruption was indicated by white arrow; the debris of *MRE* is indicated by black arrow. Scale bar, 400 nm. (**F**) The NPN fluorescence test demonstrating the BLKR treatment influenced the membrane integrity of *MRE*. $n = 3$, violin plot. (**G**) Membrane depolarization of *MRE* measured by $DiSC_3(5)$ probe. $n = 3$, mean ± SD. (**H**) Representative Bio-EM images of *MRE* (white arrow, membrane disruption). Scale bar, 500 nm. (**I**) Scheme illustrating peptide treatment for *MRE*-induced ALI. (**J**) The plotting of pulmonary *MRE* burden after indicated administration, $n = 6$, mean ± SD. (**K**) NEU counts in plasma. Each dot represents data from one mouse, $n = 5$. *P* value was calculated by comparing BLKR group with Saline group at each time point. (**L**) Representative H&E staining images of lung (0.5× field for wide view, scale bar, 2.5 mm; 20× field for enlarged region, scale bar, 100 μm). (**M**) The survival rate. $n = 15$. (**N** and **O**) The IL-6 (N) and IL-4 (O) concentration in BALF on day 6. $n = 6$, mean ± SD. Statistical analysis was conducted using one-way ANOVA.

Furthermore, the clinical available antibiotic, ceftazidime required at least three consecutive days of parenteral systemic administrations (six doses) to reach the similar pulmonary *MRE* eradication rate as SPRAY-BLKR-NP group reached on day 1 (fig. S37, A and B). Thus, the promising pulmonary *MRE* eradication allowed SPRAY-BLKR-NPs to reach nearly 80% survival rate in the first 2 days (Fig. 6M). In contrast, the 2-day survival rate of mice received LKR and ceftazidime only reached 20 and 58.3%, respectively.

SPRAY-BLKR-NPs inhibit the progression of pulmonary injury by switching the inflammation status

The exclusive anti-*MRE* therapy usually fails to rescue the mice with pulmonary *MRE* infection. Once the peptide lysed the *MRE*, the remains of bacterial cell walls containing LPS or other toxins would successively raise the secretion of proinflammatory cytokines, resulting in exacerbating lung injury. Thus, an add-on therapeutic effect, inflammation reversal, is waiting to be valid for trial on SPRAY-BLKR-NPs.

We primarily focused on the fluctuation of neutrophil levels to track the mitigation of overall inflammatory conditions. The hematology results indicated that SPRAY-BLKR-NPs successfully forestalled the neutrophil mobilization as merely 2.28 K μl^{-1} plasma neutrophils, at least twofold less than the level in mice received LKR. On day 6, the surviving mice treated with SPRAY-BLKR-NPs showed similar plasma neutrophil counts as day 1, while neutrophil concentration slightly decreased in the LKR group to 4.24 K μl^{-1} (Fig. 6K). Similar mitigation can be found in the plasma leukocyte counts (fig. S34). Such mitigation in the proinflammatory status is also proven by the decrease in BALF IL-6 level (Fig. 6N). The number of infiltrated cells is almost identical in the alveoli of all groups on day 2 (fig. S35) but much less in the alveoli of nanoparticle group on day 6 (Fig. 6L). In comparison, the six doses of ceftazidime show less capacity than our nanoparticle in inhibiting inflammation progress, testified by the significantly slower drop of BALF IL-6 and plasma neutrophil counts during therapy (fig. S37, C and D).

To investigate whether SPRAY-BLKR-NPs accelerate the establishment of anti-inflammatory microenvironment, we briefly measured the IL-4 level in BALF. The IL-4 in the SPRAY-BLKR-NP group is nearly twofold larger than the level in the LKR group by reaching 127 pg ml^{-1} (Fig. 6O), suggesting that the immune surroundings favored tissue regeneration. Hence, the edema and infiltrated cell is nearly diminished only in the alveoli of mice received SPRAY-BLKR-NPs on day 10 (fig. S36). Notably, such accelerated construction anti-inflammatory environment was not seen in Ceftazidime group (fig. S37, E to G). Our survival rate monitoring could also support this conclusion. SPRAY-BLKR-NPs reached the final 73.3% 10-day survival rate, suggesting that less than 7% of mice later died because of the following toxin-induced lung injury, while only 20 and 13.7% of mice survived in LKR group and Saline group on day 10, respectively (Fig. 6M).

DISCUSSION

The ineffectiveness of antimicrobial and anti-inflammatory pharmacotherapy in GNB-induced ALI messages the urgency to develop a single-molecule–based therapeutic for suppressing proinflammatory reactions, combating bacterial infection and constructing a regenerative environment. This work conceived a previously unidentified category of an anti-inflammatory peptide molecule, SPRAY, and screened out BLKR as the optimal candidate for immuno-programming in macrophages. In molecular engineering, we conjugate essential MPM motif to a minimalistic anti-inflammatory sequence, LKR, which constitutes crucial membrane disruption and self-assembly ability to form nanoparticles. In undifferentiated macrophage, MPM enhances cellular uptake and cytoplasmic release of anti-inflammatory sequence, amplifies the anti-inflammatory signaling transduction, and diminishes the cellular sensitivity to the proinflammatory toxin to potentiate the M2 polarization. In GNB, the MPM participates in the lysis of cells by disrupting bacterial membrane.

When treating aseptic ALI, the direct deposition of SPRAY-BLKR-NPs in the lower respiratory tract was demonstrated to rapidly mitigate neutrophil infiltration and then facilitate the regeneration of alveolar epithelium via the proliferation of M2 macrophage. When used in bacterial ALI, we also proved its promising efficacy in eradicating invading bacteria in lung. Besides, SPRAY-BLKR-NPs do not affect the monocyte migration to pulmonary interstitium or cause epithelial injury. Thus, it could be regarded as a safe inhalant for potential clinical usage. Furthermore, the peptide candidate may be used as a dry-powder inhalant or nebulized.

Overall, this work is a proof of concept that a single-molecule–based therapeutic could actualize anti-inflammation, regeneration, and antibacteria synchronously to reverse ALI with various etiologies and pathogenesis. This clinically unseen molecule may authorize the reverse of proinflammatory state in other acute inflammation, such as meningitis, arthritis, and endophthalmitis. Moreover, the chemically accessible design of SPRAY could be tailored and extended to regulate the fate of the other immune cells via MPM-induced cytoplasmic delivery of particular functional motifs.

MATERIALS AND METHODS

Materials

The following materials were used: RPMI 1640 culture medium (no. 11875093, Gibco), mouse IL-4 recombinant protein (no. BMS338, eBioscience), mouse IL-10 recombinant protein (no. 417-ML, R&D Systems), mouse macrophage colony-stimulating factor (M-CSF) protein (no. 315-02-1MG, PeproTech), LPS (no. L2630, Sigma-Aldrich), and avibactam (no. A128068, Aladdin). Peptides were synthesized and purified by GL Biochem (Shanghai) Ltd. via the Fmoc solid-phase peptide synthesis (SPPS) (*52*). Biphenyl was conjugated to N terminus using 4-biphenylacetic acid (no. 196487, Sigma-Aldrich) during the SPPS. *MRE* and *MRSA* USA300 were a gift from L. Tan, Wuhan Union Hospital, China. *K. pneumoniae* (*KP*) BNCC358281 was a gift from D. Zhou, Southern Medical University, China. *P. aeruginosa* (*PA*) PAO1 was the gift from X. Sun, Zhejiang University of Technology, China.

The isolation and culture of BMDMs

The BMDMs were extracted and cultured according to previous literature report (*53*). In short, BMDMs were isolated from the bone marrow of 6-week-old BALB/c mice (Shanghai SLAC Laboratory Animal Co. Ltd.) and further cultured in RPMI 1640/10% fetal bovine serum (FBS)/M-CSF (10 ng ml^{-1}) before the further experiment.

M2 macrophage polarization induced by SPRAY candidates

To evaluate the M2 macrophage polarization induced by peptide candidates, 2×10^5 BMDMs per well were seeded into a 12-well plate and incubated for 24 hours. The peptide candidates were added to the medium to the final concentration of 16 μM and then incubated for

48 hours. The positive control of the M2 macrophage phenotype was prepared by adding IL-4 (20 ng ml^{-1}) and IL-10 (20 ng ml^{-1}). The positive control of M1 macrophage was prepared by adding LPS (10 ng ml^{-1}) and IFN-γ (20 ng ml^{-1}). Blank medium was set as the negative control. The BMDMs were firstly blocked with anti-CD16/CD32 (no. 553141, BD Pharmingen) and stained with Fixable Viability Stain 780 (no. 565388, BD Pharmingen), anti–F4/80-BV421 (no. 123132, BioLegend), anti–CD11b-FITC (no. 557396, BD Pharmingen), anti–CD206-APC (no. 17-2061-82, eBioscience), and anti–CD86-PE (no. 553692, BD Pharmingen) according to the manufacturer's instructions. The percentages of CD206- and CD86-positive cells were then measured by a flow cytometry analyzer (CytoFLEX LX, Beckman Coulter).

Cytocompatibility assay of SPRAY candidates

Beas-2B (CRL-9609), HEK293T (CRL-3216), THP-1 (TIB-202), and RAW264.7 (TIB-71) were purchased from the American Type Culture Collection. DC 2.4 (SCC142) was purchased from Sigma-Aldrich. HS-5 (CC4028) was purchased from the Cellbook. All the cells were cultured in a 100-mm precoated dish (430167, Corning) according to the manufacturer's instructions with 10% FBS and 1% penicillin-streptomycin (no. 15140122, Gibco). To evaluate the cytocompatibility, 1×10^4 cells were seeded into the 96-well plate per well and incubated for 24 hours. Then, the medium was replaced with fresh medium containing each peptide at different concentrations. The cell viability was measured using 3-(4,5-Dimethylthiazol-2-yl)-2,5-Diphenyltetrazolium Bromide (MTT) assay after 24-hour coincubation.

Hemolysis assay of SPRAY candidates

Peptide candidates were dissolved in phosphate-buffered saline (PBS) to 512 μM, and then six times twofold dilution was performed. Ten times dilution was performed on 2 ml of freshly drawn New Zealand rabbit blood using PBS. Then, the RBC pellet was collected by centrifugation and washed eight times with PBS before incubating with peptide at different concentrations for 3 hours, 37°C. Positive control was set using 1% Triton X-100. Negative control was set using PBS. The mixture was centrifuged at 10,000 rpm, 10 min, and the absorbance at 570 nm of supernatant was measured for further hemolysis rate evaluation.

Material characterization

Chirascan V100 CD spectrometer (Applied Photophysics) was used to measure the CD spectra. LKR and BLKR were dissolved in ultrapure water (pH = 7.4) to the concentration of 128 μM and then subjected to CD spectrum recording.

The CMC value of the peptide was revealed by a spectrofluorometer (Edinburgh, F55). LKR and BLKR were dissolved in PBS (2.56 mM) and then underwent eight twofold dilutions. The pH suspension was adjusted to 7. Peptide suspension (100 μl) was mixed with 2 μl of Rhodamine 6G (final concentration: 5 μM), then incubated for 24 hours. The wavelength with maximum optical density (OD) value (515 to 560 nm) was read out for CMC calculation.

The morphology of peptide assemblies was imaged by Talos L120C G2 transmission electron microscope (Thermo Fisher Scientific). LKR and BLKR were dissolved in PBS (128 μM), then preincubated for 8 hours. Suspension (10 μl) was applied on 200-mesh copper grids, followed by 2-min uranyl acetate staining before TEM imaging.

To monitor the stability of SPRAY-BLKR-NPs in injured alveolar environment, BALF was extracted from ALI mice at 24 hours after LPS (10 mg kg^{-1}) administration. The SPRAY-BLKR-NPs were then incubated ALI BALF to the final concentration of 256 μM. The diameter of nanoparticle at indicated incubation time was measured by a BI-200SM NanoBrook ZetaPALS analyzer using number distribution mode.

To perform the accelerated storage testing for SPRAY, 1.5 mg of BLKR powder was placed in 2-ml glass vial and then incubated under low temperature (4°C, sealed), light exposure (4500 K, 25°C, sealed), high temperature (60°C, unsealed), or high humidity (90% relative humidity, 37°C, unsealed) for 10 days using medicine Stability Testing Chamber (LHH-150GSD, Blue pard, Shanghai). After incubation, the peptide powder was checked for appearance, and reconstituted particle size in PBS was measured by DLS. The chemical purity was measured by high-performance liquid chromatography (Agilent).

The uptake behavior of SPRAY in BMDMs

The cellular distribution of peptide was analyzed by a confocal laser scanning microscope (LSM 800, Zeiss). A total of 2×10^5 BMDMs were seeded into a 20-mm glass bottom cell culture dish (no. 801001, NEST) and then incubated respectively with FITC-labeled LKR and BLKR for indicated time points. The nuclei were stained with Hoechst 33342 (no. 62249, Thermo Fisher Scientific), and the lysosomes were stained with LysoTracker Deep Red (L12492, Thermo Fisher Scientific) according to the manufacturer's instructions. Then, the cells were washed with PBS three times and cultured in live cell imaging solution (A14291DJ, Thermo Fisher Scientific) for further CLSM imaging (Zeiss LSM 980).

Flow cytometry was used to reveal the cellular uptake behavior of BLKR. To evaluate cellular uptake quantity, FITC-labeled LKR and BLKR were coincubated with 10^6 BMDMs for 1 hour and then washed with PBS five times for further quantification using flow cytometry.

To quantify the cellular uptake molar level of BLKR, BWLR, and BVRR, 10^6 BMDMs per well were seeded into a six-well plate and incubated for another 24 hours, then incubated with BLKR, BWLR, and BVRR (final concentration: 16 μM) in RPMI 1640 culture medium (10% FBS) for 1 hour. Ultrapure water (1 ml) was added to each well and incubated for 20 min to lyse the cells by hypotonicity. The suspension containing cell lysate was lyophilized, followed by adding 400 μl of methanol and ultrasonication to dissolve the peptide. The resuspended cell lysate was centrifuged at 10,000 rpm for 5 min. The supernatant was filtered by a 220-nm filter and then analyzed through the Agilent 1260 InfinityLab Liquid Chromatography system equipped with InfinityLab Poroshell 120 EC-C8 column (4.5 mm by 100 mm, 2.7 μm, no. 695975-906, Agilent Technologies).

The method to evaluate the endocytosis mode was previously described (*52*). Briefly, 10^6 BMDMs were seeded into a 12-well plate and then preincubated with single or blended uses of endocytosis inhibitors for 30 min, respectively. The medium was discarded, and fresh medium containing FITC-labeled BLKR was added to each well to the final concentration of 16 μM with the presence of indicated inhibitors, followed by 15-min coincubation. The percentage of $BLKR^+$ cells and mean fluorescence intensity were further quantified by flow cytometry. In each coincubation, the final concentrations of various indicated inhibitors were applied at 5 mM for MβCD, 50 μM for Amiloride, 50 μM for EIPA, 40 μM for CPZ and 5 μg ml^{-1} for Filipin III.

Bio-EM (Talos L120C G2 transmission electron microscope) was used to provide direct visualization of the peptide's endocytosis

process and cytoplasmic releasing. A total of 1×10^6 BMDMs were incubated in a 12-well plate and then treated by BLKR (16 μM, PBS) for 15 min, 1 hour, 2 hours, and 4 hours. PBS was used as the negative control. Then, the medium was discarded, and the cells were gently scraped off with the presence of 900 μl of PBS and 100 μl of FBS and centrifuged. The cell pellet was fixed with fixation buffer (2.5% glutaraldehyde) and then subjected to embedding, staining, and imaging according to the instructions from Westlake Electron Microscopy Core Facility.

BMDMs polarization study induced by the optimal SPRAY

CLSM imaging was used to reveal the CD206 expression and morphological change in BMDMs. A total of 2×10^5 BMDMs were cultured in glass bottom cell culture dish and then incubated with LKR and BLKR (16 μM) for 24 hours, respectively. Cells were fixed with 4.2% paraformaldehyde for 10 min and penetrated using 0.1% Triton 100-X for 5 min, then blocked with the blocking solution containing 1% BSA and 10% goat serum for 1 hour. The anti-MMR/CD206 (no. AF 2535, R&D Systems) was applied at the final concentration of 0.25 μg for 10^6 cells and incubated overnight at 4°C. The AF488-AffiniPure Donkey Anti-Goat IgG (no. 705-545-147, Jackson ImmunoResearch) was then applied at 2 μg for 10^6 cells. The cells were then stained with 4′,6-diamidino-2-phenylindole (DAPI) and subjected to CLSM imaging.

To evaluate the inflammatory-related mRNA expression levels of the BMDM cells after being stimulated with peptide for 24 hours, the total RNA was extracted with TRIzol (no. 15596018, Thermo Fisher Scientific), then quantified using NanoDrop (Thermo Fisher Scientific), the mRNA was purified, and cDNA was prepared using one NovoScript 1st Strand cDNA Synthesis SuperMix (gDNA Purge) Kit (E047-01B, Novoprotein). The real-time PCR was then performed subsequently in triplicate using NovoStart SYBR qPCR SuperMix Plus Kit (E096-01B, Novoprotein) and a Bio-Rad CFX96 real-time PCR system. The relative expression of mRNA was normalized to the expression level of GAPDH.

ELISA was used to measure the cytokines secreted by BMDMs. A total of 1×10^6 BMDMs were seeded in a 6-well plate and then incubated with LKR and BLKR (16 μM) for 24 hours with 1 ml of culture media. The supernatant was collected for analyzing the concentration of IL-4 (no. BMS613, Thermo Fisher Scientific), IL-10 (no. BMS614, Thermo Fisher Scientific), IL-5 (no. 431201, BioLegend), TNF-α (no. 430904, BioLegend) and IFN-γ (no. 430815, BioLegend), respectively, according to manufacturer's protocol.

To investigate the effect of peptide pretreatment, BMDMs were incubated with LKR and BLKR (16 μM) for 24 hours. Then the medium was not discarded. LPS (10 ng ml^{-1}) and IFN-γ (20 ng ml^{-1}) were added to each well, incubated for another 24 hours, and then subjected to the flow cytometry analysis.

Transcriptome sequencing for macrophage polarization

A total of of 5×10^6 BMDMs were incubated with LKR and BLKR (16 μM) for 48 hours. RNA extraction was performed using TRIzol Reagent (no. 15596026, Invitrogen) according to the manufacturer's instructions. Genomic DNA was removed using DNase I (no. 2270B, Takara). Library construction and RNA sequencing were completed at Shanghai Majorbio Bio-pharm Biotechnology Co., Ltd. (Shanghai, China) according to the manufacturer's instructions (Illumina, San Diego, CA). The expression level of each gene was calculated according to the transcripts per million reads (TPM). Significantly different expressed genes were considered to be slog2 (fold change) $| \geq 1$ and P-adjust ≤ 0.05 (DESeq2). The GO (www.geneontology.org) and KEGG (www.genome.jp/kegg/) pathway enrichment analysis was carried out using Majorbio Cloud Platform (www.majorbio.com).

Bactericidal activity of SPRAY

The MIC values of peptide against *MRE*, *PA* and *KP* were measured according to previously reported method (*54*). Ceftazidime (no. 72558-82-8, Yuanye, Shanghai) and imipenem (GP11075, Glpbio) were used as positive control.

To investigate *MRE* viability after peptide treatment. *MRE* (1×10^7 CFU ml^{-1}, PBS) in mid-logarithmic growth-phase was incubated with LKR and BLKR (128 μM) for 4 hours at 37°C. Then, 10 μl of mixture was transferred then quantified to reveal bacterial viability using spread-plate method. The method to evaluation the *MRSA* viability was the same as aforementioned steps, but *MRSA* (1×10^8 CFU ml^{-1}, PBS) in mid-logarithmic growth-phase was used. Untreated bacteria were used as control group.

To investigate the anti-*MRE* activity of BLKR in the healthy and injured alveolar environment. Healthy BALF was extracted from untreated mice using 1 ml of cold sterile PBS. To extract ALI BALF, 8-week-old BALB/c mice received LPS (10 mg kg^{-1}) followed by BALF extraction at 24 hours later using 1 ml of cold PBS. The BALF was sonicated for 5 min to lysed living cells before further use. Then, *MRE* (1×10^7 CFU ml^{-1}) in mid-logarithmic growth-phase was resuspended using freshly extracted healthy BALF and ALI BALF and incubated with LKR and BLKR for 4 hours (128 μM) at 37°C. Then, 10 μl of mixture was transferred then quantified to reveal bacterial viability using spread-plate method.

Living/Dead staining was performed to visualize the biofilm eradication induced by peptides. In short, to culture the biofilm, 200 μl of *MRE* or *MRSA* (5×10^6 CFU ml^{-1}) was preincubated for 48 hours using LB medium. Then, the LB medium was replaced by PBS containing. The biofilm was then incubated with LKR and BLKR (256 μM, PBS) for 4 hours at 37°C. The biofilm was then stained using LIVE/DEAD BackLight bacterial viability kit (Invitrogen) and processed with CLSM imaging (Zeiss LSM 800).

To visualize the bactericidal phenotype of SPRAY, *MRE* and *MRSA* (1×10^8 CFU ml^{-1}) were preincubated on a 12-mm round glass slide in a 12-well plate for 48 hours. Then, the bacteria were washed with PBS three times and further incubated with LKR and BLKR (256 μM) for 3 hours. Next, the bacteria were washed with PBS three times before fixed 2.5% glutaraldehyde for 24 hours. The imaging process using SEM (FE-SEM, GeminiSEM 450) and Bio-EM (Talos L120C G2) was performed at Westlake Electron Microscopy Core Facility.

SPRAY-induced bacterial membrane disruption

NPN uptake assay was performed to prove the bacterial membrane integrity altered by peptide treatment. NPN test solution (10 μl; 1 mM) was coincubated with *MRE* or *MRSA* suspension (1×10^8 CFU ml^{-1}, 5 mM glucose, 5 mM Hepes, pH = 7.4) at 0 min. Then, peptide was added to the final concentration of 256 μM at 30 min after the NPN addition, followed by coincubation for 2 hours. Triton X-100 (1%) was used as the positive control. The fluorescence intensity (excitation: 350 nm, emission: 420 nm) was then measured by spectrofluorometer (Edinburgh, F55).

Membrane-potential-sensitive dye $DiSC_3(5)$ was used to investigate bacterial Membrane depolarization. *MRE* or *MRSA* (100 μl;

2×10^8 CFU ml^{-1}, 20 mM glucose, 5 mM Hepes, 0.1 mM KCl, pH = 7.4) with $DiSC_3(5)$ (20 nM) addition at 0 min was mixed with an equal volume of LKR or BLKR (512 μM) at 1 min. The fluorescence intensity (excitation: 622 nm, emission: 670 nm) of the mixture was then measured every minute using spectrofluorometer (Edinburgh, F55) for the following 29 min starting from the time point of peptide addition.

To evaluate the conformational changes during the peptide-membrane interaction, PE, PG, and DPG were mixed at the proportion of 79:17:4 in chloroform (final lipid concentration is 5 mM) to mimic the composition of GNB membrane (*55*). The lipid solution was then fired by N_2 flow and resuspended using ultrapure water, then extruded through 0.1-μm pore polycarbonate membrane 15 times using AvantiMini Extruder (Alabaster). The resulting LNPs (1 mM) were then incubated with BLKR (128 μM) for 30 min before the CD measurement.

Mice studies

All mice studies were approved by the Institutional Animal Care and Use Committee of Westlake University (AP#22-079-WHM). Eight-week-old BALB/c mice were purchased from Shanghai SLAC Laboratory Animal Co. Ltd. Mice were anesthetized with the intraperitoneal injection of 2.5% Avertin at 18 to 20 μl g^{-1} before each nonlethal surgery or operation.

Immunomodulatory function and toxicity of SPRAY in healthy mice

Mice (n = 3) received twice doses of SPRAY-BLKR-NPs (50 μl) through intratracheal injection at the concentration of 64, 128, 256, 512, and 1024 μM, respectively. The time gap between each injection was set as 12 hours. Then, the mice were euthanized at 24 hours after last BLKR administration. Blood was collected through retro-orbital blood collection and then analyzed using ProCyte Dx Hematology Analyzer (IDEXX). for hematology assay. The main organs were collected for H&E staining for the acute toxicity examination.

To investigate the monocyte infiltration in the lung parenchyma, freshly collected lungs that received the treatment above were ground, filtered, lysed for 60 min using lung lysis buffer according to previous report (*56*). RBCs were lysed before staining. The dispersed pulmonary cells were cultured in RPMI 1640 medium for another 4 hours and then stained with anti–CD45-BUV395 (no. 564279, BD Pharmingen), anti–CD64a-BV650 (no. 740622, BD Pharmingen), anti–MERTK-BV786 (no. 747890, BD Pharmingen), CD11b-FITC (no. 561688, BD Pharmingen) for further flow cytometry analysis.

Long-term safety evaluation of the consecutive administrations of SPRAY nanoparticles

Mice received twice doses of SPRAY-BLKR-NPs (256 μM, 50 μl, 0.76 mg kg^{-1}) for consecutive 14 days. The time gap between each injection was set as 12 hours. Then, the mice were raised for another 13 days. To investigate the leukocyte infiltration, hemolysis and anemia, blood samples were collected on days 3, 6, 9, 12, 15, 21, and 27 through retro-orbital blood collection, and then analyzed Hematology Analyzer for WBC and RBC parameters. To evaluate potential liver and kidney side effects, blood samples were centrifuged at 4000 rpm for 10 min to obtain the serum, then subjected to AST, ALT, ALP, and BUN analysis using automatic biochemical analyzer (Catalyst one, IDEXX). To evaluate the lung function, trachea was exposed by blunt separation, then 18G needle was intubated into trachea and tied by suture. After the trachea was connected with ventilator, the lung function test was performed on invasive computer-controlled piston ventilator (FlexiVent; SCIREQ Inc.) on days 6, 15, and 27. Then, BALF was extracted for IL-4 and IL-6 measurement using ELISA. The main organs were collected on day 27 for H&E staining.

SPRAY nanoparticles reverse LPS-induced ALI in mice

For modeling of LPS-induced ALI, LPS was administrated through intratracheal injection at 10 mg kg^{-1}. To monitor the biodistribution of SPRAY in ALI lung and healthy lung, FITC-labeled BLKR and FITC-labeled LKR (128 μM, 50 μl) were administrated locally in mice (n = 3) through intratracheal injection at 12 after LPS administration. The body weight was monitored daily. Mice were euthanized at indicated time point, and lungs were collected for perfusion using PBS and embedded in the OCT, then stored at −80°C. Lung was cryosectioned using Leica CM3050 S Research Cryostat and stained with ProLong Diamond Antifade Mountant with DAPI (P36966, Thermo Fisher Scientific) before CLSM imaging. To further visualize the colocalization of SPRAY with macrophage, lung sections were further stained with anti-CD68 (no. 14-0681-82, Thermo Fisher Scientific), AF647 secondary antibody (no. A-21247, Thermo Fisher Scientific) and DAPI, then subjected to CLSM imaging.

To investigate the uptake distribution of SPRAY nanoparticles in lung immune cells, ALI mice received SPRAY-BLKR-NPs (128 μM, 50 μl) locally. At 1 hour after administration, lung was harvested, ground, filtered, lysed then stained with viability staining blue (no. L23105, Invitrogen), anti–CD45-APC-Cy7 (no. 557659, BD Pharmingen), anti–CD3-PE-Cy5.5 (no. 100274, BioLegend), anti–F4/80-BV421 (no. 123132, BioLegend), anti–Ly6G-APC (no. 560599, BD Pharmingen), anti–CD19-BV605 (no. 563148, BD Pharmingen) and anti–CD11c-PE (no. 12-0114-82, eBioscience) for flow cytometry analysis.

In the therapy process, LKR and BLKR (128 μM, 50 μl) were administrated locally in mice (n = 3) through intratracheal injection at 12 and 24 hours after LPS injection. BALF was extracted on days 0, 2, 4, and 6 according to previous literature report (*57*). The blood was harvested through retro-orbital blood collection. The hematology parameters and leukocyte differential counting in blood and BALF were then measured using ProCyte Dx Hematology Analyzer (IDEXX). ELISA test was used to measure the cytokines level in BALF. BALF (n = 5) was centrifuged at 500g for 10 min. The concentrations of IL-6 (no. MU30044, Bioswamp) and IL-4 (no. MU30385, Bioswamp) in the supernatant were analyzed according to the manufacturer's protocol.

For the pulmonary histological analysis, mice were euthanized on days 0, 2, 4, and 6 using CO_2. The lung was harvested, perfused, and embedded in paraffin, then sectioned for H&E staining. The counts of inflammatory cells in alveoli were calculated from nine randomly selected H&E staining sections; n = 3 mice per group, three sections per mouse were selected.

To screen the therapeutic dosage range of SPRAY for treating aseptic ALI, ALI mice were dosed with optimal SPRAY locally every 12 hours two times at indicated dosage at day 1. The therapeutic efficacy for tissue regeneration was measured by the BALF IL-4 level on day 6.

The immunofluorescence and IHC analysis in ALI mice

The paraffin sections were firstly dehydrated gradient using ethanol-water solution and xylene. Then, the slides were incubated with sodium citrate antigen retrieval solution (no. C1032, Solarbio) and 3%

hydrogen peroxide. The immunostaining for SFTPC-positive type II pneumocytes was performed using SFTPC Polyclonal Antibody (Proteintech, no. 10774-1-AP) at 1:2000 dilution rate, then followed by the previously described methods (*58*). Slides were scanned using a digital pathology imaging system (KFBIO, KF-pro-400). The percentage of SFTPC-positive cells was quantified on QuPath-0.2.3 using the positive cell detection function (threshold 1: 0.18, threshold 2: 0.3, threshold 3: 0.4). Twelve randomly selected images (20× field) from three mice (four images per mouse) were analyzed in quantification. The immunofluorescence staining of CD206-positive and CD86-positive macrophages was performed using anti-CD86 (no. MA1-10299, Thermo Fisher Scientific) at 1:500. The secondary antibody for CD86 was applied using AF647-Goat anti-Rat IgG (no. A-21247, Thermo Fisher Scientific) at 1:500. Anti-MMR/CD206 (no. AF 2535, R&D Systems) was then applied at 1:1000. The secondary antibody for CD206 was applied using AF488-AffiniPure Donkey Anti-Goat IgG (no. 705-545-147, Jackson ImmunoResearch) at 1:500. Nuclei were stained with DAPI and subjected to CLSM imaging. To quantify the percentage of CD86-positive cells or CD206-positive cells among total pulmonary cell counts, up to 12 randomly selected images (20× field) and measured using QuPath-0.2.3 with the fluorescence mode. $n = 3$ mice per group, at least 5 images per mouse were selected.

Pharmacokinetic study of SPRAY-BLKR-NPs

ALI mice received single dose of SPRAY-BLKR-NPs (256 μM, 50 μl; 18.42 μg per mouse), then euthanized at predetermined time points. The main organs were harvested. Lung tissues were harvested after cardiac perfusion using 10 ml of cold PBS. To measure the BLKR content, the tissues were lyophilized and crushed into powder with a mortar and pestle. The dry weight of tissue was measured. Then, the crushed tissue was suspended using the mixture of chloroform and methanol (volume ratio = 1:3) followed by freeze grinding at 30 Hz 10 times with the assistance of two steel grinding beads (⌀3.2 and ⌀5.2 mm) using a bullet blender (JXFSTPRP-II, Shanghai Jinxin). The homogenized tissue was centrifuged at 14,000 rpm for 3 min. The supernatant was filtered by 220 nm filter, then analyzed through Agilent 1260 InfinityLab Liquid Chromatography system using InfinityLab Poroshell 120 EC-C18 column (4.5 mm by 50 mm, 2.7 μm, no. 699975-902, Agilent Technologies).

Liver microsomal metabolism of SPRAY

The metabolic rate of SPRAY in human, dog, monkey, rat, and mouse liver microsomes was measured by Shanghai Medicilon Inc. BLKR (1 μM) was coincubated with human (bioreclamationIVT), monkey, dog, rat, and mouse liver microsomes (Xenotech) (0.75 mg ml^{-1}), respectively. Mixed solution of peptide and microsomes (30 μl) was then mixed with 15 μl of NADPH stocking solution (6 mM), and incubation for indicated period. Subsequently, 150 μl of stop solution (ACN: MeOH = 1:1) containing internal standard (tolbutamide) was added to stop the reaction. The suspension was oscillated for 10 min (600 rpm) and centrifuged at 6000 rpm for 15 min. The supernatant was diluted 2.5-fold with pure water for further LC/MS analysis.

SPRAY nanoparticles reverse inflammation in GNB-infected mice

A total of 2.5×10^7 CFU *MRE* per mouse was locally administrated through intratracheal injection at day 0 to model *MRE* infection-induced ALI. Mice received the local administration of LKR and BLKR (256 μM, 50 μl) at 12, 24, 36, and 48 hours through intratracheal injection, respectively. To monitor the survival rate, 45 mice were randomly divided into three groups ($n = 15$) followed by pulmonary *MRE* infection as previously described. The survival rate was monitored daily until day 6. Mice were euthanized on days 2, 6, and 10 using CO_2. The lung was harvested, perfused, and embedded, then subjected to H&E staining. BALF supernatant was collected using the method above and then subjected to an ELISA test for IL-6 and IL-4 concentration. The hematology study was analyzed using the blood collected through retro-orbital bleeding.

GNB eradication of SPRAY nanoparticles in mice

To investigate the in vivo anti-*MRE* efficiency of BLKR. Mice received the intratracheal injection of 2.5×10^7 CFU *MRE* at day 0. Peptide was administrated through intratracheal injection injection at 12 and 24 hours after infection. Saline (0.9%) was used as the negative control. Then, the entire lung was collected in a sterile 5-ml EP tube at 6 hours after each dosing. Sterile PBS (2 ml) was added, and the lung was homogenized with a handheld homogenizer (Tenlin-A, China) for 30 s. Using the spread-plate method, 20 μl of lung homogenate was immediately transferred for *MRE* quantification.

To screen the therapeutic dosage range of SPRAY for treating GNB-induced ALI, *MRE*-infected mice were dosed with optimal SPRAY locally every 12 hours four times at indicated dosage. Pulmonary *MRE* burden was investigated at 12 hours after the final dosing. Lung tissue was collected on day 6, then subjected to H&E staining. Survival rate was monitored throughout the experiment.

To compare the therapeutic efficacy of SPRAY-BLKR-NPs with clinically available antibiotic, *MRE*-infected mice ($n = 5$) received the local administration of SPRAY-BLKR-NPs (256 μM, 50 μl, 0.76 mg kg^{-1}) and subcutaneous injection of ceftazidime/avibactam (32/8 mg kg^{-1}) (*59*, *60*), respectively, every 12 hours six times. The lung was collected at 12 hours after second and sixth administration, then homogenized for pulmonary *MRE* quantification. Blood samples were collected on days 1, 5, and 9 for neutrophil quantification using Hematology Analyzer. The IL-4 and IL-6 levels in BALF were measured using ELISA on days 1 and 5 to investigate the alternation of alveolar immuno-microenvironment. Survival rate was monitored throughout the experiment. Lung tissue was collected on day 5, then subjected to H&E staining.

Supplementary Materials

This PDF file includes:

Figs. S1 to S40
Tables S1 to S5

REFERENCES AND NOTES

1. M. A. Matthay, R. L. Zemans, G. A. Zimmerman, Y. M. Arabi, J. R. Beitler, A. Mercat, M. Herridge, A. G. Randolph, C. S. Calfee, Acute respiratory distress syndrome. *Nat. Rev. Dis. Primers.* **5**, 18 (2019).
2. M. J. D. Griffiths, D. F. McAuley, G. D. Perkins, N. Barrett, B. Blackwood, A. Boyle, N. Chee, B. Connolly, P. Dark, S. Finney, A. Salam, J. Silversides, N. Tarmey, M. P. Wise, S. V. Baudouin, Guidelines on the management of acute respiratory distress syndrome. *BMJ Open Respir. Res.* **6**, e000420 (2019).
3. L. B. Ware, M. A. Matthay, The acute respiratory distress syndrome. *N. Engl. J. Med.* **342**, 1334–1349 (2000).
4. J. A. Whitsett, T. Alenghat, Respiratory epithelial cells orchestrate pulmonary innate immunity. *Nat. Immunol.* **16**, 27–35 (2015).
5. E. Fan, D. M. Needham, T. E. Stewart, Ventilatory management of acute lung injury and acute respiratory distress syndrome. *JAMA* **294**, 2889–2896 (2005).
6. E. Kyriazopoulou, G. Poulakou, H. Milionis, S. Metallidis, G. Adamis, K. Tsiakos, A. Fragkou, A. Rapti, C. Damoulari, M. Fantoni, I. Kalomenidis, G. Chrysos, A. Angheben, I. Kainis,

Z. Alexiou, F. Castelli, F. S. Serino, M. Tsilika, P. Bakakos, E. Nicastri, V. Tzavara, E. Kostis, L. Dagna, P. Koufargyris, K. Dimakou, S. Savvanis, G. Tzatzagou, M. Chini, G. Cavalli, M. Bassetti, K. Katrini, V. Kotsis, G. Tsoukalas, C. Selmi, I. Bliziotis, M. Samarkos, M. Doumas, S. Ktena, A. Masgala, I. Papanikolaou, M. Kosmidou, D.-M. Myrodia, A. Argyraki, C. S. Cardellino, K. Koliakou, E.-I. Katsigianni, V. Rapti, E. Giannitsioti, A. Cingolani, S. Micha, K. Akinosoglou, O. Liatsis-Douvitsas, S. Symbardi, N. Gatselis, M. Mouktaroudi, G. Ippolito, E. Florou, A. Kotsaki, M. G. Netea, J. Eugen-Olsen, M. Kyprianou, P. Panagopoulos, G. N. Dalekos, E. J. Giamarellos-Bourboulis, Early treatment of COVID-19 with anakinra guided by soluble urokinase plasminogen receptor plasma levels: A double-blind, randomized controlled phase 3 trial. *Nat. Med.* **27**, 1752–1760 (2021).

7. K. A. Rodvold, J. M. George, L. Yoo, Penetration of anti-infective agents into pulmonary epithelial lining fluid: Focus on antibacterial agents. *Clin. Pharmacokinet.* **50**, 637–664 (2011).
8. M. Exner, S. Bhattacharya, B. Christiansen, J. Gebel, P. Goroncy-Bermes, P. Hartemann, P. Heeg, C. Ilschner, A. Kramer, E. Larson, W. Merkens, M. Mielke, P. Oltmanns, B. Ross, M. Rotter, R. M. Schmithausen, H.-G. Sonntag, M. Trautmann, Antibiotic resistance: What is so special about multidrug-resistant Gram-negative bacteria? *GMS Hyg. Infect. Contr.* **12**, Doc05 (2017).
9. P. M. Lepper, T. K. Held, E. M. Schneider, E. Bölke, H. Gerlach, M. Trautmann, Clinical implications of antibiotic-induced endotoxin release in septic shock. *Intensive Care Med.* **28**, 824–833 (2002).
10. J. Liu, S. Zhang, X. Dong, Z. Li, Q. Xu, H. Feng, J. Cai, S. Huang, J. Guo, L. Zhang, Y. Chen, W. Zhu, H. Du, Y. Liu, T. Wang, L. Chen, Z. Wen, D. Annane, J. Qu, D. Chen, Corticosteroid treatment in severe COVID-19 patients with acute respiratory distress syndrome. *J. Clin. Invest.* **130**, 6417–6428 (2020).
11. C. Guo, B. Li, H. Ma, X. Wang, P. Cai, Q. Yu, L. Zhu, L. Jin, C. Jiang, J. Fang, Q. Liu, D. Zong, W. Zhang, Y. Lu, K. Li, X. Gao, B. Fu, L. Liu, X. Ma, J. Weng, H. Wei, T. Jin, J. Lin, K. Qu, Single-cell analysis of two severe COVID-19 patients reveals a monocyte-associated and tocilizumab-responding cytokine storm. *Nat. Commun.* **11**, 3924 (2020).
12. L. A. Ritter, N. Britton, E. L. Heil, W. A. Teeter, S. B. Murthi, J. H. Chow, E. Ricotta, D. S. Chertow, A. Grazioli, A. R. Levine, The impact of corticosteroids on secondary infection and mortality in critically ill COVID-19 patients. *J. Intensive Care Med.* **36**, 1201–1208 (2021).
13. D. Khanna, C. J. F. Lin, D. E. Furst, B. Wagner, M. Zucchetto, G. Raghu, F. J. Martinez, J. Goldin, J. Siegel, C. P. Denton, Long-term safety and efficacy of tocilizumab in early systemic sclerosis-interstitial lung disease: Open-label extension of a Phase 3 randomized controlled trial. *Am. J. Respir. Crit. Care Med.* **205**, 674–684 (2022).
14. T. Hussell, T. J. Bell, Alveolar macrophages: Plasticity in a tissue-specific context. *Nat. Rev. Immunol.* **14**, 81–93 (2014).
15. Z. Tu, Y. Zhong, H. Hu, D. Shao, R. Haag, M. Schirner, J. Lee, B. Sullenger, K. W. Leong, Design of therapeutic biomaterials to control inflammation. *Nat. Rev. Mater.* **7**, 557–574 (2022).
16. T. Harel-Adar, T. B. Mordechai, Y. Amsalem, M. S. Feinberg, J. Leor, S. Cohen, Modulation of cardiac macrophages by phosphatidylserine-presenting liposomes improves infarct repair. *Proc. Natl. Acad. Sci. U.S.A.* **108**, 1827–1832 (2011).
17. W. Tian, X. Jiang, R. Tamosiuniene, Y. K. Sung, J. Qian, G. Dhillon, L. Gera, L. Farkas, M. Rabinovitch, R. T. Zamanian, M. Inayathullah, M. Fridlib, J. Rajadas, M. Peters-Golden, N. F. Voelkel, M. R. Nicolls, Blocking macrophage leukotriene B_4 prevents endothelial injury and reverses pulmonary hypertension. *Sci. Transl. Med.* **5**, 200ra117 (2013).
18. J. Han, Y. S. Kim, M. Y. Lim, H. Y. Kim, S. Kong, M. Kang, Y. W. Choo, J. H. Jun, S. Ryu, H. Y. Jeong, J. Park, G. J. Jeong, J. C. Lee, G. H. Eom, Y. Ahn, B. S. Kim, Dual roles of graphene oxide to attenuate inflammation and elicit timely polarization of macrophage phenotypes for cardiac repair. *ACS Nano* **12**, 1959–1977 (2018).
19. P. P. P. S. J. Khedoe, X. Wu, R. Gosens, P. S. Hiemstra, Repairing damaged lungs using regenerative therapy. *Curr. Opin. Pharmacol.* **59**, 85–94 (2021).
20. J. Hu, T. Wei, H. Zhao, M. Chen, Y. Tan, Z. Ji, Q. Jin, J. Shen, Y. Han, N. Yang, L. Chen, Z. Xiao, H. Zhang, Z. Liu, Q. Chen, Mechanically active adhesive and immune regulative dressings for wound closure. *Matter* **4**, 2985–3000 (2021).
21. Y. Zhang, S. Wang, Y. Yang, S. Zhao, J. You, J. Wang, J. Cai, H. Wang, J. Wang, W. Zhang, J. Yu, C. Han, Y. Zhang, Z. Gu, Scarless wound healing programmed by core-shell microneedles. *Nat. Commun.* **14**, 3431 (2023).
22. G. Fredman, N. Kamaly, S. Spolitu, J. Milton, D. Ghorpade, R. Chiasson, G. Kuriakose, M. Perretti, O. Farokzhad, I. Tabas, Targeted nanoparticles containing the proresolving peptide Ac2-26 protect against advanced atherosclerosis in hypercholesterolemic mice. *Sci. Transl. Med.* **7**, 275ra20 (2015).
23. F. Wang, Q. Huang, H. Su, M. Sun, Z. Wang, Z. Chen, M. Zheng, R. W. Chakroun, M. K. Monroe, D. Chen, Z. Wang, N. Gorelick, R. Serra, H. Wang, Y. Guan, J. S. Suk, B. Tyler, H. Brem, J. Hanes, H. Cui, Self-assembling paclitaxel-mediated stimulation of tumor-associated macrophages for postoperative treatment of glioblastoma. *Proc. Natl. Acad. Sci. U.S.A.* **120**, e2204621120 (2023).
24. N. Mookherjee, M. A. Anderson, H. P. Haagsman, D. J. Davidson, Antimicrobial host defence peptides: Functions and clinical potential. *Nat. Rev. Drug Discov.* **19**, 311–332 (2020).
25. H. Chu, M. Pazgier, G. Jung, S. P. Nuccio, P. A. Castillo, M. F. de Jong, M. G. Winter, S. E. Winter, J. Wehkamp, B. Shen, N. H. Salzman, M. A. Underwood, R. M. Tsolis, G. M. Young, W. Lu, R. I. Lehrer, A. J. Baumler, C. L. Bevins, Human α-defensin 6 promotes mucosal innate immunity through self-assembled peptide nanonets. *Science* **337**, 477–481 (2012).
26. L. A. Haines-Butterick, D. A. Salick, D. J. Pochan, J. P. Schneider, In vitro assessment of the pro-inflammatory potential of β-hairpin peptide hydrogels. *Biomaterials* **29**, 4164–4169 (2008).
27. M. Wan, A. M. van der Does, X. Tang, L. Lindbom, B. Agerberth, J. Z. Haeggstrom, Antimicrobial peptide LL-37 promotes bacterial phagocytosis by human macrophages. *J. Leukoc. Biol.* **95**, 971–981 (2014).
28. A. M. Smith, R. J. Williams, C. Tang, P. Coppo, R. F. Collins, M. L. Turner, A. Saiani, R. V. Ulijn, Fmoc-diphenylalanine self assembles to a hydrogel via a novel architecture based on π–π interlocked β-sheets. *Adv. Mater.* **20**, 37–41 (2008).
29. R. A. Shah, T. W. Ostertag, S. Tang, T. D. Dziubla, J. Z. Hilt, Development of biphenyl monomers and associated crosslinked polymers with intramolecular pi-pi interactions. *J. Appl. Polym. Sci.* **138**, 50257 (2021).
30. W. Kim, W. Zhu, G. L. Hendricks, D. Van Tyne, A. D. Steele, C. E. Keohane, N. Fricke, A. L. Conery, S. Shen, W. Pan, K. Lee, R. Rajamuthiah, B. B. Fuchs, P. M. Vlahovska, W. M. Wuest, M. S. Gilmore, H. Gao, F. M. Ausubel, E. Mylonakis, A new class of synthetic retinoid antibiotics effective against bacterial persisters. *Nature* **556**, 103–107 (2018).
31. J. K. Martin II, J. P. Sheehan, B. P. Bratton, G. M. Moore, A. Mateus, S. H.-J. Li, H. Kim, J. D. Rabinowitz, A. Typas, M. M. Savitski, M. Z. Wilson, Z. Gitai, A dual-mechanism antibiotic kills gram-negative bacteria and avoids drug resistance. *Cell* **181**, 1518–1532 e14 (2020).
32. L. Schnaider, S. Brahmachari, N. W. Schmidt, B. Mensa, S. Shaham-Niv, D. Bychenko, L. Adler-Abramovich, L. J. W. Shimon, S. Kolusheva, W. F. DeGrado, E. Gazit, Self-assembling dipeptide antibacterial nanostructures with membrane disrupting activity. *Nat. Commun.* **8**, 1365 (2017).
33. A. de Breij, M. Riool, R. A. Cordfunke, N. Malanovic, L. de Boer, R. I. Koning, E. Ravensbergen, M. Franken, T. van der Heijde, B. K. Boekema, P. H. S. Kwakman, N. Kamp, A. El Ghalbzouri, K. Lohner, S. A. J. Zaat, J. W. Drijfhout, P. H. Nibbering, The antimicrobial peptide SAAP-148 combats drug-resistant bacteria and biofilms. *Sci. Transl. Med.* **10**, eaan4044 (2018).
34. J. S. Suk, Q. Xu, N. Kim, J. Hanes, L. M. Ensign, PEGylation as a strategy for improving nanoparticle-based drug and gene delivery. *Adv. Drug Deliv. Rev.* **99**, 28–51 (2016).
35. M. Liu, S. Hu, N. Yan, K. D. Popowski, K. Cheng, Inhalable extracellular vesicle delivery of IL-12 mRNA to treat lung cancer and promote systemic immunity. *Nat. Nanotechnol.* **19**, 565–575 (2024).
36. T. M. John, A. Deshpande, K. Brizendine, P.-C. Yu, M. B. Rothberg, Epidemiology and outcomes of community-acquired *Escherichia coli* pneumonia. *Open Forum Infect. Dis.* **9**, ofab597 (2021).
37. T. A. Russo, Z. Wang, B. A. Davidson, S. A. Genagon, J. M. Beanan, R. Olson, B. A. Holm, P. R. Knight III, P. R. Chess, R. H. Notter, Surfactant dysfunction and lung injury due to the *E. coli* virulence factor hemolysin in a rat pneumonia model. *Am. J. Physiol. Lung Cell Mol. Physiol.* **292**, L632–L643 (2007).
38. C. Porta, M. Rimoldi, G. Raes, L. Brys, P. Ghezzi, D. Di Liberto, F. Dieli, S. Ghisletti, G. Natoli, P. De Baetselier, A. Mantovani, A. Sica, Tolerance and M2 (alternative) macrophage polarization are related processes orchestrated by p50 nuclear factor kappaB. *Proc. Natl. Acad. Sci. U.S.A.* **106**, 14978–14983 (2009).
39. S. J. Forbes, N. Rosenthal, Preparing the ground for tissue regeneration: From mechanism to therapy. *Nat. Med.* **20**, 857–869 (2014).
40. T. Yu, S. Gan, Q. Zhu, D. Dai, N. Li, H. Wang, X. Chen, D. Hou, Y. Wang, Q. Pan, J. Xu, X. Zhang, J. Liu, S. Pei, C. Peng, P. Wu, S. Romano, C. Mao, M. Huang, X. Zhu, K. Shen, J. Qin, Y. Xiao, Modulation of M2 macrophage polarization by the crosstalk between Stat6 and Trim24. *Nat. Commun.* **10**, 4353 (2019).
41. R. S. McHugh, M. J. Whitters, C. A. Piccirillo, D. A. Young, E. M. Shevach, M. Collins, M. C. Byrne, $CD4^+CD25^+$ immunoregulatory T cells: Gene expression analysis reveals a functional role for the glucocorticoid-induced TNF receptor. *Immunity* **16**, 311–323 (2002).
42. A. Gutiérrez-González, M. Martínez-Moreno, R. Samaniego, N. Arellano-Sánchez, L. Salinas-Muñoz, M. Relloso, A. Valeri, J. Martínez-López, Á. L. Corbí, A. Hidalgo, Á. García-Pardo, J. Teixidó, P. Sánchez-Mateos, Evaluation of the potential therapeutic benefits of macrophage reprogramming in multiple myeloma. *Blood* **128**, 2241–2252 (2016).
43. R. Xu, Y. Li, H. Yan, E. Zhang, X. Huang, Q. Chen, J. Chen, J. Qu, Y. Liu, J. He, Q. Yi, Z. Cai, CCL2 promotes macrophages-associated chemoresistance via MCPIP1 dual catalytic activities in multiple myeloma. *Cell Death Dis.* **10**, 781 (2019).
44. K. Sadtler, K. Estrellas, B. W. Allen, M. T. Wolf, H. Fan, A. J. Tam, C. H. Patel, B. S. Luber, H. Wang, K. R. Wagner, J. D. Powell, F. Housseau, D. M. Pardoll, J. H. Elisseeff, Developing a pro-regenerative biomaterial scaffold microenvironment requires T helper 2 cells. *Science* **352**, 366–370 (2016).

45. T. Guan, X. Zhou, W. Zhou, H. Lin, Regulatory T cell and macrophage crosstalk in acute lung injury: Future perspectives. *Cell Death Discov.* **9**, 9 (2023).
46. A. González-López, G. M. Albaiceta, Repair after acute lung injury: Molecular mechanisms and therapeutic opportunities. *Crit. Care* **16**, 209 (2012).
47. W. J. Zacharias, D. B. Frank, J. A. Zepp, M. P. Morley, F. A. Alkhaleel, J. Kong, S. Zhou, E. Cantu, E. E. Morrisey, Regeneration of the lung alveolus by an evolutionarily conserved epithelial progenitor. *Nature* **555**, 251–255 (2018).
48. A. J. Lechner, I. H. Driver, J. Lee, C. M. Conroy, A. Nagle, R. M. Locksley, J. R. Rock, Recruited monocytes and type 2 Immunity promote lung regeneration following pneumonectomy. *Cell Stem Cell* **21**, 120–134.e7 (2017).
49. R. Mourtada, H. D. Herce, D. J. Yin, J. A. Moroco, T. E. Wales, J. R. Engen, L. D. Walensky, Design of stapled antimicrobial peptides that are stable, nontoxic and kill antibiotic-resistant bacteria in mice. *Nat. Biotechnol.* **37**, 1186–1197 (2019).
50. P. Domenico, W. G. Johanson Jr., D. C. Straus, Lobar pneumonia in rats produced by clinical isolates of Klebsiella pneumoniae. *Infect. Immun.* **37**, 327–335 (1982).
51. O. H. Robertson, L. T. Coggeshall, E. E. Terrell, Experimental pneumococcus lobar pneumonia in the dog. *J. Clin. Invest.* **12**, 467–493 (1933).
52. H. Wang, Z. Feng, Y. Wang, R. Zhou, Z. Yang, B. Xu, Integrating enzymatic self-assembly and mitochondria targeting for selectively killing cancer cells without acquired drug resistance. *J. Am. Chem. Soc.* **138**, 16046–16055 (2016).
53. J. Weischenfeldt, B. Porse, Bone marrow-derived macrophages (BMM): Isolation and applications. *CSH Protoc.* **2008**, pdb.prot5080 (2008).
54. CLSI, *Methods for Dilution Antimicrobial Susceptibility Tests for Bacteria That Grow Aerobically; Approved Standard-Eighth Edition* (Clinical and Laboratory Standards Institute, M07-A8, 2009).
55. A. W. Simonson, A. S. Mongia, M. R. Aronson, J. N. Alumasa, D. C. Chan, A. Lawanprasert, M. D. Howe, A. Bolotsky, T. K. Mal, C. George, A. Ebrahimi, A. D. Baughn, E. A. Proctor, K. C. Keiler, S. H. Medina, Pathogen-specific antimicrobials engineered de novo through membrane-protein biomimicry. *Nat. Biomed. Eng.* **5**, 467–480 (2021).
56. J. Schyns, Q. Bai, C. Ruscitti, C. Radermecker, S. De Schepper, S. Chakarov, F. Farnir, D. Pirottin, F. Ginhoux, G. Boeckxstaens, F. Bureau, T. Marichal, Non-classical tissue monocytes and two functionally distinct populations of interstitial macrophages populate the mouse lung. *Nat. Commun.* **10**, 3964 (2019).
57. L. Van Hoecke, E. R. Job, X. Saelens, K. Roose, Bronchoalveolar lavage of murine lungs to analyze inflammatory cell infiltration. *J. Vis. Exp.* **123**, 55398 (2017).
58. A. Liu, X. Zhang, R. Li, M. Zheng, S. Yang, L. Dai, A. Wu, C. Hu, Y. Huang, M. Xie, Q. Chen, Overexpression of the SARS-CoV-2 receptor ACE2 is induced by cigarette smoke in bronchial and alveolar epithelia. *J. Pathol.* **253**, 17–30 (2021).
59. J. Berkhout, M. J. Melchers, A. C. van Mil, S. Seyedmousavi, C. M. Lagarde, W. W. Nichols, J. W. Mouton, Pharmacokinetics and penetration of ceftazidime and avibactam into epithelial lining fluid in thigh- and lung-infected mice. *Antimicrob. Agents Chemother.* **59**, 2299–2304 (2015).
60. P. Levasseur, A.-M. Girard, L. Lavallade, C. Miossec, J. Pace, K. Coleman, Efficacy of a ceftazidime-avibactam combination in a murine model of septicemia caused by Enterobacteriaceae species producing AmpC or extended-spectrum β-lactamases. *Antimicrob. Agents Chemother.* **58**, 6490–6495 (2014).

Acknowledgments: We thank the Instrumentation and Service Center for Molecular Sciences, Instrumentation and Service Center for Physical Sciences, and Biomedical Research Core Facilities at Westlake University for assistance with measurements. We thank S. Li for the help in peptide synthesis. **Funding:** This work was supported by the National Natural Science Foundation of China (82272145 and 82022038) to H.W. **Author contributions:** Conceptualization: H.W. Methodology: D.C., J.L., B.W., X.Y., and H.W. Investigation: D.C., Z.Z., N.K., T.X., J.L., P.X., B.Y., Y.Z., Y.S., Y.L., X.Y., and H.W. Validation: D.C., Z.Z., N.K., J.L., B.Y., and Y.S. Resources: D.C., Y.S., and H.W. Formal analysis: D.C. and H.W. Visualization: D.C. and H.W. Data curation: D.C. and H.W. Project administration: H.W. Supervision: H.W. Funding acquisition: H.W. Writing—original draft: D.C. and H.W. Writing—review and editing: D.C. and H.W. **Competing interests:** H.W., D.C., Z.Z., and N.K. have fielded a patent converting this work. All the other authors declare that they have no competing interests. **Data and materials availability:** All data needed to evaluate the conclusions in the paper are present in the paper and/or the Supplementary Materials.

Submitted 19 January 2024
Accepted 8 August 2024
Published 13 September 2024
10.1126/sciadv.ado1749